Hydrodynamics of Advanced High–Speed Sealift Vessels

Leo Victor Lazauskas

Thesis submitted for the degree of
Master of Science
in
Applied Mathematics
at
The University of Adelaide
(Faculty of Engineering, Computer and Mathematical Sciences)

Discipline of Applied Mathematics

29 April 2005

Abstract

There is at present great interest in large ships capable of carrying substantial cargo at speeds in excess of 40 knots. At the same time, there are large gaps in our understanding of the hydrodynamics, structural engineering, and economics of high–speed vessels.

Monohulls, catamarans, trimarans, surface effect ships, and air cushion vehicles are considered in the present work. The total resistance of these vessels is divided into separate components which are estimated using different methods. Skin-friction is estimated using Grigson's algorithm which gives much better predictions of flat plate skin–friction than the traditional ITTC method. Wave resistance of displacement hulls is estimated using Michell's thin-ship theory: a similar theory is used for the wave resistance of travelling pressure distributions. Several simple formulae are derived that can be used at the preliminary design stage of catamarans to estimate optimum demihull separation.

Memetic algorithm techniques are used to find vessels with minimum (calm-water) total resistance. Optimal geometric parameters are found for vessels of 1200 tonnes under a variety of geometric limitations and constraints on upright stability, at design speeds of 50 knots and 75 knots. Estimates are made of the principal weight components of the optimal vessels. Empirical formulae for the efficiencies of powerplants and propulsors then enable estimates to be made of the maximum range, the cargo capacity, and the fuel consumption.

ADMINISTRATION

Signed Statement

This work contains no material that has been accepted for the award of any other degree or diploma in any university or other tertiary institution and, to the best of my knowledge and belief, contains no material previously published or written by another person, except where due reference has been made in the text.

I give consent to this copy of my thesis, when deposited in the University Library, being available for loan and photocopying.

Signed: Leo Victor Lazauskas

Acknowledgements

I owe great thanks to Professor Ernie Tuck, not only for sharing his expertise during the supervision of this thesis, but also for providing me with a variety of aerodynamic and hydrodynamic challenges I can enjoy well into my dotage.

The cheerful willingness of Professor Lawrence Doctors to discuss his own work in ship hydrodynamics is very much appreciated. Thanks also are due to Dr. David Scullen with whom I collaborated on other hydrodynamic projects that provided many insights for the present thesis. Mrs Dianne Parish has made all administrative contact with the Department of Applied Mathematics a delight.

My friend and colleague Dr. Brian Kirke contributed absolutely nothing to this thesis. Nonetheless, I would never have started, nor continued, in applied mathematics without his encouragement and collaboration over the last fifteen years.

I acknowledge useful discussions with my son Misha Lazauskas who introduced me to the delights of the virtual world of Avatar MUD, and to the possibilities of using artificial life techniques inside multi-player games to solve difficult engineering optimisation problems. Finally, I acknowledge useful discussions with, and directives from, Kitty Davis, who has lovingly corrected, and organised my life for almost 30 years.

NOTATION

ACRONYMS

ACV	Air Cushion Vehicle
BL	Boundary Layer
HSST	High–Speed Sealift Technology
ITTC	International Towing Tank Conference
SES	Surface Effect Ship
sfc	Specific Fuel Consumption

ROMAN SYMBOLS

A_f	Above–water frontal area of vessel
A_{wp}	Waterplane area
B	Hull beam
B_0	Log law constant in BL calculations
c_f	Planar local skin friction coefficient
C_F	Planar drag coefficient
D	Hull depth (to main deck)
E_1, E_2	Equipment numerals in structural weight estimates
F	Froude number based on ship length
g	Gravitational acceleration
$\overline{GM}_T$	Transverse metacentric height
H_f	Height of freeboard
H_s	Height of superstructure
L	Ship or hull length
p	Pressure
P_e	Effective power
P_s	Shaft power
R_n	Reynolds number
R_1	Reynolds number based on BL displacement thickness
R_2	Reynolds number based on BL momentum thickness
R_A	Air resistance
R_F	Skin friction
R_L	Equivalent lift resistance
R_M	Momentum resistance of air cushion

R_T	Total resistance
R_V	Viscous resistance
R_W	Wave resistance
s_{max}	Range
S	Hull wetted surface area
T	Hull draft
U	Ship speed
w	Distance between demihull centrelines
W	Displaced weight
W_c	Cargo weight (i.e. payload)
W_d	Deadweight
W_e	Empty ship weight
W_f	Fuel weight
W_g	Weight of gas turbine and gearboxes
W_m	Weight of machinery
W_o	Outfit weight
W_p	Weight of propulsion system
W_s	Structural weight
x, y, z	Co-ordinates of a point in the wave field

GREEK SYMBOLS

∇	Hull displacement volume
ζ	Wave elevation
η_p	Overall propulsive coefficient
θ	Wave propagation angle
κ	Von Karman constant in BL calculations
ν	Molecular kinematic viscosity
Π	Coles wake strength parameter in BL calculations
ρ	Fluid density
σ	Ratio of weight supported by sidehulls to the total ship weight
τ	Ratio of weight supported by air cushions to the total ship weight
ϕ	Disturbance velocity potential
ϖ	Wave co-ordinate: $\varpi = x\cos\theta + y\sin\theta$

Contents

1 INTRODUCTION

1.1 Motivation

Fast ships capable of transporting large payloads are needed by many commercial, military and humanitarian relief organisations. However high-speed vessels are subject to large drag forces which must be minimised (subject to many technological and operational constraints) so that the vessel can be competitive with other existing freight systems.

This need for efficiency and high speed has forced designers to be innovative because traditional single-hulled ships are not capable of satisfying all of the demands expected of them in all possible operational situations.

Despite many years of research and experimentation, the hydrodynamics of traditional monohull vessels is still not completely understood. Innovative vessels have been subject to even less scrutiny, so there are many aspects of their performance that must be investigated before they can be considered confidently for routine sea-lift operations.

Although there is the expectation that high-speed vessels will find niche markets and may be competitive with air transport, there is still doubt as to their ability to economically carry very large payloads over large distances.

It is well known that hovercraft have much lower resistance than traditional water-borne craft at high speeds. Why then are there so few hovercraft in service?

1.2 Classification of Vessels

The phrase "high-speed ship" will conjure up different images to different people and there is no universally accepted, precise, definition of the term. For Trillo [62] it depends on one's point of view:
"In the world of boats and ships the hydrodynamicist may associate it with a length-based Froude number of 1.0, regardless of vessel size, while an operator may think of it in terms of speeds of 30 knots or more."

For other hydrodynamicists, a vessel is considered to be travelling at high speed when the Froude number is greater than 0.5.

In the present thesis a "high-speed sealift vessel" is one that has a displacement of at least 1000 tonnes, and that is capable of a top speed of at least 50 knots (≈ 92 kilometres per hour).

Sea-lift vessels can be conveniently characterised according to the manner in which they remain on (or above) the surface of water.

Displacement vessels are the most common type of water craft, and what most people would associate with the term "ship". These vessels float because they displace a volume of water equal to their weight; the well-known Archimedean principle. Displacement vessels with more than one hull are called *multihulls*. *Catamarans* (from the Tamil word *kattamaran* meaning "tied trees") are two-hulled vessels. The neologisms *trimaran*, *tetramaran* and *pentamaran* are popular terms for vessels with, respectively, three, four and five hulls.

Planing vessels are displacement vessels that, in addition to buoyant forces, are also subject to dynamic forces tending to lift the hull out of the water at high speeds, much in the same way as aeroplanes are held aloft by the passage of air over their wings. In the case of planing vessels however, lift is generated by the passage of fluid only on the underside of the hull. Although they are capable of very high speeds, planing vessels are unable to carry large payloads efficiently, and their performance in waves is often poor by comparison with other vessels. We will not consider planing hulls in the present work.

Air Cushion Vehicles (ACV) are rigid platforms supported by a pressurised bubble of air generated by large fans and contained by flexible skirts. Hovercraft are the most common form of ACV. Multiple air cushion vehicles (MACV) can be thought of as analogous to displacement multihulls. They can also be viewed as vehicles with a single, non-uniform, pressure distribution acting over a rectangular region.

Surface Effect Ships (SES) are air cushion vehicles that have rigid sidewalls instead of flexible skirts. Seals installed between the sidewalls at the front and rear of the vessel assist in maintaining the pressurised air cushion which supports approximately 80% of the weight of the vessel. When operating "off-cushion", i.e. when the air-cushion pressure is zero, the behaviour of an SES can be considered as identical to that of a "pure" catamaran. If the cushion pressure is high enough to lift the sidewalls completely out of the water, the vessel can be considered as performing as a "pure" ACV.

Hydrofoil vessels are partly supported by the hydrodynamic lift of submerged wings. Although they have excellent prospects for high–speed transport primarily because of their ability to maintain high speeds in large seas, we will not consider them in the present work.

The vessels of interest in the present work are a subset of a larger family

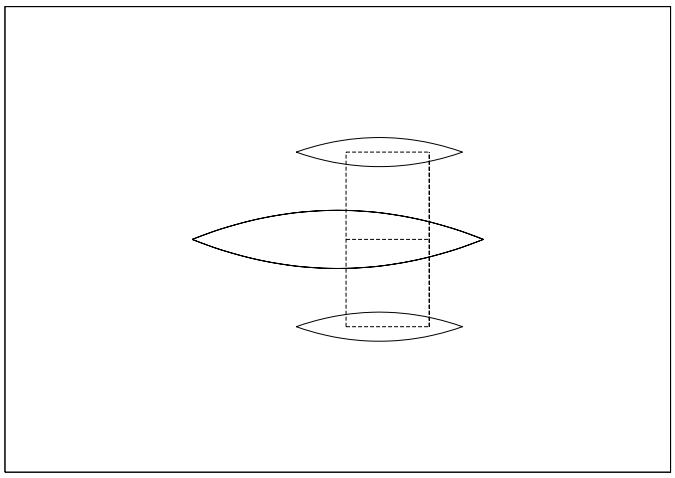

Figure 1: Layout of a generalised air-cushion supported trimaran: nominal cushion locations are indicated by the dashed lines.

of generalised air-cushion-supported trimarans. These vessels consist of a main hull together with two side hulls placed parallel to each other as shown in Figure 1. If the vessel has air-cushions they must be placed between the central hull and the outriggers as shown in the figure. The vessel geometry will be described in more detail later.

A particular member of this family of vessels can be identified uniquely by a pair of non-dimensional numbers, σ and τ, where σ is the fraction of total displacement supported by the side hulls, and τ is the fraction of total displacement supported by the air cushions.

Using this convention, "pure" displacement vessels have $\tau = 0$; a "pure" hovercraft (ACV) has $\sigma = 0$. Other vessels of interest are given in Table 1.

In the present thesis we will not consider vessels with a central hull as well as air-cushions, i.e. all SES have $\sigma \equiv 1.0$.

1.3 Background

The development of vessels capable of carrying large payloads efficiently at high speed has proceeded via what seems like small, incremental advances over thousands of years. By the mid 1950s, the largest high–speed displacement vessels were probably naval destroyers with top speeds of about

Vessel	σ	τ
Monohull	0	0
Catamaran	1	0
Trimaran	$0 < \sigma < 1$	0
SES	$0 < \sigma < 1$	$0 < \tau < 1$
ACV	0	1

Table 1: Members of a family of generalised air-cushion supported trimarans. σ is the fraction of total displacement supported by sidehulls; τ is the fraction of total displacement supported by air cushions.

40 knots. Sir Christopher Cockerell's invention of the hovercraft suddenly opened up a huge gap between what was practicable for displacement vessels, which are ultimately limited by their very high frictional resistance, and what was possible if that component of resistance was eliminated.

In my opinion, the high-speed ship industry has been trying, ever since, to fill in the gap between traditional monohull displacement vessels and hovercraft, with a variety of hybrid vessels. Very slender monohull vessels are known to have low total resistance but they are laterally unstable, and have very small areas available for cargo: multihull vessels can, to a greater or lesser degree, ameliorate these problems. Similarly, hovercraft have well-known problems with directional stability and excessive power requirements to maintain the air cushion pressure: Surface Effect Ships, (or captured air bubble vehicles as they were known then, [13]), were developed by A.G. Ford and others around 1964, in an attempt to improve some of the problems faced by ACV. Doctors [13] survey of the research conducted on the hydrodynamics of travelling pressure distributions contains a valuable list of references tracing the development of air-cushion vehicles.

With so many possible vessel types, how is a naval architect to decide on the best, or at least the best subset, of vessels?

Ship hydrodynamics, too, seemed to progress slowly and incrementally over the 2,000 years separating Archimedes and William Froude (1810–1879). Michell's [47] landmark paper in 1898 on the wave resistance of a ship, and its subsequent rediscovery by Havelock [32] in 1923, heralded a new era in ship hydrodynamics. With Michell's analytic theory for the wave resistance

problem in hand, researchers finally had a method, if not efficient computational methods and machines, with which to approach resistance minimisation problems. For an account of Michell's influence on ship hydrodynamics see Tuck [66].

The earliest attempts at finding hullforms with minimum wave resistance seem to have been made by Weinblum in 1930, and more formally by Pavlenko in 1937: see Wehausen [83] for an extensive history of the search for ships of minimum resistance. These early attempts were valuable for the insights they gave, however the actual hullforms generated by the various optimisation systems were, on the whole, impractical as they were characterised by large corrugations in the hull waterplanes.

More recently, Doctors and Day [17], and Tuck and Lazauskas [68], began using stochastic algorithms to find hullforms and multihull arrangements of minimum total resistance. Doctors and Day [17] allowed all offsets of their hulls to vary independently during the optimisation process. As earlier workers had also found, the optimal hull forms had impractical corrugations. Tuck and Lazauskas [68] used a parameterisation of the hull in their first optimisation study. The optimal hulls found during the study were very long, slender, canoe-like bodies: impractical, perhaps, for real ocean–going ships, but quite reasonable as rowing shells or as the central hull of a trimaran. The parameterised approach was generalised to monohulls and catamarans by Doctors and Day [16], and to generalised trimarans by Lazauskas and Tuck, [39].

In a more mathematical optimisation study, Lazauskas and Tuck, [41] and Tuck and Lazauskas, [70] considered several multihull arrangements including monohulls, catamarans, trimarans, and tetramarans, as well as the so–called *Weinblum* catamarans which are comprised of two longitudinally–staggered demihulls. The latter study also considered the far-field wave elevations of the vessels. Multihull arrangements were found that had extremely low wave resistance (and very low wave-making) for some speed ranges. An arrangement with four hulls in a diamond pattern was found to have very low wave resistance at relatively low speeds, but the vessel was impractically long and the vessel was not competitive with others considered in the study when frictional resistance was included.

Early work on the minimisation of wave resistance of travelling pressure distributions was undertaken by, among others, Maruo [42] and Bessho [2]. Newman and Poole [50] compared the wave resistance of rectangular and of elliptical planforms.

Doctors and Day, [18] recently optimised unconstrained families of pressures, in which a large rectangular pressure distribution was divided into subcushions, [79]. Tuck and Lazauskas [72] optimised both unconstrained and constrained pressure distributions with up to 4000 parameters, with indications of convergence toward a continuous optimum, [79]. Although distributions were found that had very low wave resistance, they were completely impractical. Pressure variations throughout the distribution were smooth, but fluctuations were very large, varying from -160kPa to 275kPa. It is unlikely that standard seals could contain such large pressures. More unexpectedly, estimated wave elevations under the distribution were found to vary from 37m in some troughs up to 26m at the largest crest!

It is not difficult to spot a recurring theme in the above potted history of the search for ships of minimum resistance: mathematically optimal vessels seem, almost inevitably, to be impractical for one reason or another. Certainly, valuable insights have been gained as a result of the research but, outside of small towing tank models, not one of these "optimal" vessels has ever been built.

Clearly, the search for ships of minimum resistance should be conducted with practical engineering constraints in mind, however the constraints that would guarantee a buildable high–speed ship are not yet fully understood.

The 1997 HSST Workshop [53] was a landmark event in high-speed ship design. Attended by more than 200 delegates from academia, government, and industry, the workshop made technology projections that should be available by 2002 and also by about 2010. The impact of those technology projections on transport performance was assessed quantitatively which provided insights into the transport potential of hullforms and other technologies of interest.

It was claimed [53, p. vii], that the quantitative methods used at the HSST Workshop to assess candidate vessel types were based on "first principle physics", but it is not clear what the term implies. The 1999 report by Lavis and Forstell [37] describes a physics–based model called "PASS (Parametric Analysis of Ship Systems)" which grew out of the HSST Workshop and was developed with the assistance of the U.S. Navy. The report gives only scant details of the algorithms used in the program but they admit that [37, p. 4], "In no case, however, are the algorithms completely without empiricism". The model uses the ITTC line (or similar, it is not clear) for the skin friction, but is silent on the method used to predict wave resistance or any other resistance components.

Broadbent and Kennell [3], used a similar design tool to "PASS" in their analysis of the capabilities of monohulls, catamarans, trimarans and SES. To estimate the resistance of monohulls they used a standard hull series approach with the well-known Series 64 hull as a basis. The friction component of resistance in their program was, "...corrected to ITTC from ATTC predictions". For catamarans, they used interpolation on a set of test results published by Molland et al [48] for vessels with a different hullform, namely the NPL series. Their method for estimating the resistance of trimarans is almost completely opaque:

> "Trimaran resistance estimate is based mainly on the centre hull resistance. For the side hull to main hull interference, ... the user is allowed to influence the calculation of the beneficial interference between the trimaran main hull and side hulls. ...The user selects a percentage of the between hull wave energy that can be recovered from proper placement of the side hulls. This estimate is based on comparison of the design sidehull location with external predictions of interference margins. This fraction of the sidehull resistance is then removed from the entire resistance, this limited to 50% of the sidehull wavemaking resistance and for the sidehull arrangement used here, is usually set at 50% of this setting."

1.4 Objective

The objective of the present thesis can be thought of as a preliminary ship design problem, the central task being to optimise, and then to compare, the performance of a variety of vessels which meet certain practical and geometric criteria.

As measures of "performance", we consider the powering requirements, fuel consumption, payload, and range of the vessels for two design speeds, namely 50 knots and 75 knots.

2 GEOMETRY

2.1 Multihull Geometry

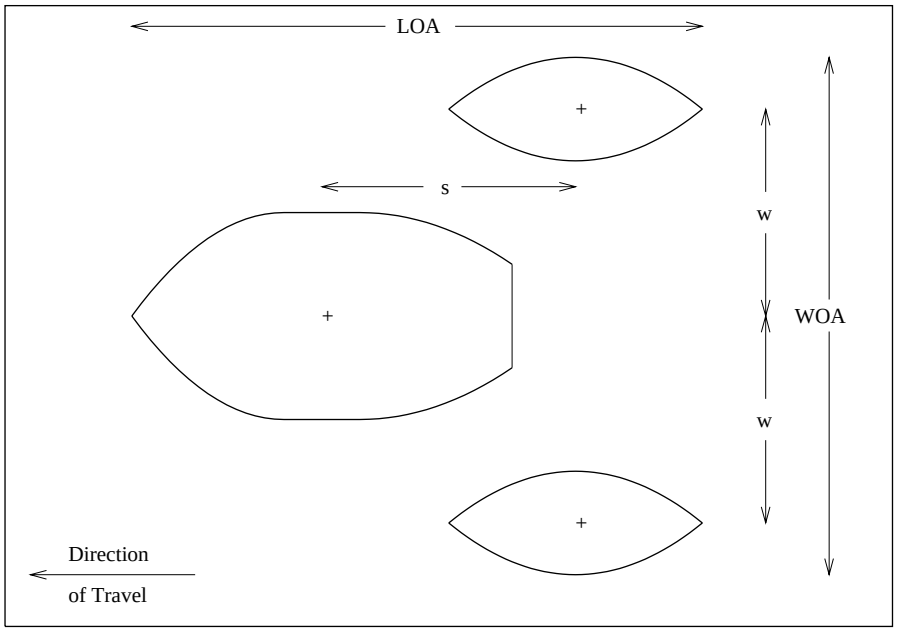

Figure 2: Plan view of a generalised trimaran.

For the purposes of the work, a generalised trimaran is regarded as a central hull together with two side hulls placed parallel to each other with their centres at a distance s aft of the centre of the central hull, and at distances w abeam of the central hull, as shown in Figure 2.

If the displacement of the central hull is equal to zero, the ship is a laterally symmetric catamaran; when the outriggers have displacements both equal to zero, the ship is a monohull.

The co-ordinate system is such that the negative x-axis is in the direction of travel; the positive y-axis is to starboard, and z increases upwards from the undisturbed free surface which is the plane $z = 0$. The co-ordinate origin in the x, y-plane is the centre of the central hull.

In the present thesis the sidehulls are not allowed to extend beyond the bow or stern of the central hull.

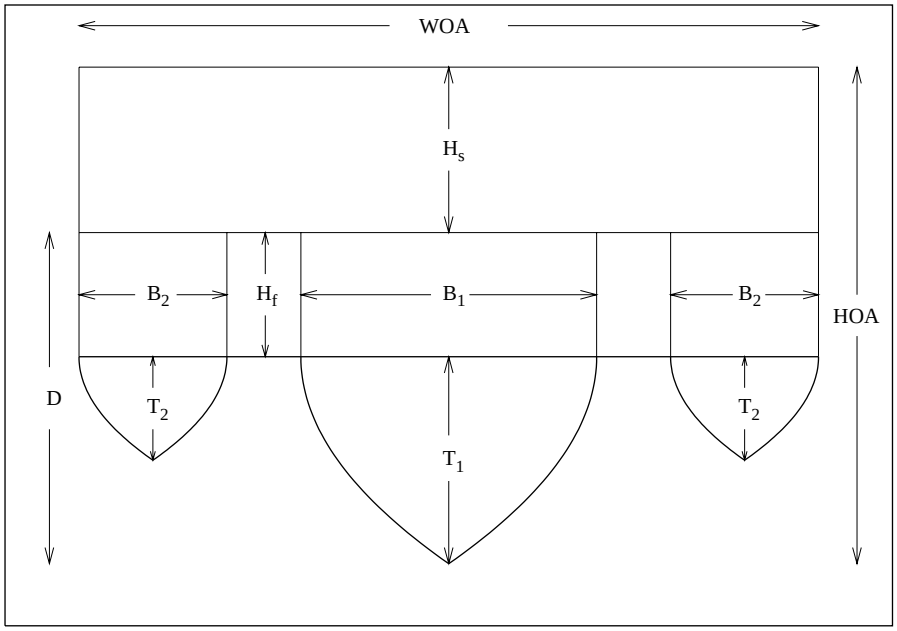

Figure 3: Section view of a generalised trimaran.

2.2 Hybrid Vessel Geometry

A "hybrid vessel" is a laterally symmetric multihull vessel that may or may not have additional air cushions. Air-cushions are assumed to be of rectangular planform and located so that they are enclosed at the sides by the demihulls of the vessel. The cushions cannot extend beyond the bows or the sterns of the sidehulls that enclose them.

2.3 Hull Geometry

All hullforms used in the present study come from the same eight-parameter mathematical family. The present series is an extension of a three-parameter series used in previous work by Tuck and Lazauskas, e.g. [68],[39].

We first consider the forebody shape, which is defined by three shape parameters. In the present thesis, all three parameters are constrained to lie between 0.0 and 1.0, inclusive. The hull series is such that if a parameter has value 0.0, then the relevant shape is rectangular; 0.5 corresponds to an

Hull	f_0	f_1	f_2	f_3	f_4	f_5	f_6	f_7
Rectangular Strut	0.0	0.0	0.0	0.0	0.0	0.5	0.5	0.0
Elliptic Strut	0.5	0.0	0.0	0.5	0.0	0.5	0.5	0.0
Parabolic Strut	1.0	0.0	0.0	1.0	0.0	0.5	0.5	0.0
Wigley	1.0	1.0	0.0	1.0	0.0	0.5	0.5	0.0
PEP (Canoe-like)	1.0	0.5	1.0	1.0	1.0	0.5	0.5	0.0
Hemisphere	0.5	0.5	0.5	0.5	0.5	0.5	0.5	0.0
Lego 1	1.0	1.0	0.0	0.0	0.0	1.0	1.0	0.5
Lego 5	1.0	1.0	0.0	1.0	0.0	0.5	0.0	1.0

Table 2: Some representative hulls of an eight-parameter hull series.

elliptical shape, and 1.0 creates a parabolic shape. Intermediate values will produce shapes intermediate between these familiar shapes. For example, a value of 0.25 for a parameter indicates that the resultant shape will be fuller than elliptical, but not as full as a rectangle.

Let $X(x) = 4x(1-x)$, with $0 \leq x \leq 1$. Then the non-dimensional offsets, $Y = Y(x, z; f_0, f_1, f_2)$, are given by $Y = 0$ if $X = 0$ or if $X^{f_2} < z$. Otherwise $Y = 1/2FG^{f_1}$. Here $F = X^{f_0}$, $G = 1 - z^2X^{-2f_2}$ and $0 \leq x, z, f_0, f_1, f_2 \leq 1$.

In the above formulation, the first parameter, f_0, controls the shape of the waterlines, the second parameter, f_1, determines the cross-section shape, and the third parameter, f_2, controls the shape of the keel-line.

The shape of the afterbody is defined in a similar fashion. Here, however, we do not need to define a cross-section shape because, for a clean join, the forebody and the afterbody cross-sections must be identical. The afterbody waterplane shape is given by the parameter f_3, the afterbody buttock shape is f_4.

The last three parameters in the series determine the relative length of the forebody and the afterbody, and the transom size.

Shape parameter f_5 determines the relative length of the forebody. Thus, the hull entry length is given by $L_E = f_5L$, where L is the hull length. The relative length of the afterbody is determined by the value of parameter f_6, and the length of the run is therefore $L_R = f_6L$.

If $f_5 + f_6 < 1$ then the hull has a parallel middlebody of relative length $1 - f_5 - f_6$. The actual length of the parallel middle body is $L - L_E - L_R$.

The final parameter, f_7, is the "transom stern cut-off ratio". If $f_7 = 0$, there is no transom stern, i.e. the afterbody is not truncated. If $f_7 > 0$ then the afterbody is truncated, but the relative length of the afterbody is unchanged and is still given by f_6. For example, if $f_7 = 0.25$, then one quarter of the afterbody is cut off to form a transom stern.

At any given length and draft, we adjust the beam by uniform scaling of the non-dimensional offsets given by the above formulae, so as to achieve the desired displacement.

The series contains several shapes commonly encountered in ship design. For example, a "standard" Wigley hull is a fore-aft symmetric vessel with parabolic waterlines and cross-sections, and rectangular buttocks; the non-dimensional offsets are given by the set of eight parameters, $\{1, 1, 0, 1, 0, 0.5, 0.5, 0\}$. A fore-aft symmetric, parabolic strut can be formed using the set, $\{1, 0, 0, 1, 0, 0.5, 0.5, 0\}$.

Note that our eight-parameter series includes as special cases the "Lego" hulls of Doctors and Day [19].

In the present thesis we have constrained the shape parameters to lie between 0 and 1 which ensures that waterlines, cross-sections and buttocks are convex. Although concave and reflexed shapes can be formed by allowing some parameters to take values greater than 1, this was found to lead to undesirable results in many cases. For example, optimal hulls would often have very cusped waterlines and buttocks.

Figure 4 shows three views of one member of the hull family. In the waterplane view at the top of the figure, B is the beam of the hull, i.e. the maximum width of the hull, and B_t, is the width of the stern. The overall length of the hull, L, is the sum of the length of the entry, L_E, the length of the parallel middlebody, L_P, and the length of the run, L_R. Hull parameter f_0 controls the shape of the forebody waterlines; f_3 determines the shape of the afterbody waterlines.

In the sideview shown in the middle of Figure 4, the overall height of the hull HOA can be seen to be the sum of the draft, T, the freeboard, H_f, and the superstructure, H_s. The hull depth, D, is the sum of the draft and the freeboard. T_t is the draft of the stern section. Hull parameters f_2 and f_4 control, respectively, the keel-lines of the forebody and afterbody.

In the cross-section view shown at the bottom of Figure 4, f_1 controls the shape of the hull-sections. Although the underwater (curved) portion of the hull and the vertical, above-water portion form a continuous curve, there can be a discontinuity in the derivatives at the intersection of the two portions.

2.4 Pressure Distribution Geometry

In the present thesis we will consider only constant pressure distributions of rectangular planform.

There are well-known ([13], [24], [61]) numerical difficulties associated with constant pressure distributions but these generally occur at low Froude numbers. In particular, it has been found that a sudden pressure fall-off around the perimeter of the distribution causes unrealistically large humps and hollows in the wave resistance curve at low Froude numbers.

Several methods to ameliorate the problem have been proposed. Doctors and Sharma [20] employed a hyperbolic pressure distribution of the form

$$\begin{aligned} p(x,y) = \frac{1}{4}\{&\tanh\left[\alpha(x+L_p/2)\right] - \tanh\left[\alpha(x+L_p/2)\right]\} \\ &\times\{\tanh\left[\beta(y+B_p/2)\right] - \tanh\left[\beta(y+B_p/2)\right]\} \end{aligned} \tag{1}$$

where α and β are *smoothing parameters*. Delhommeau [10] has also used this distribution in more recent work. It can be seen that the distribution extends to infinity in both the x and y directions. The special case $\alpha, \beta \to \infty$ corresponds to a uniform pressure of finite extent.

Wilson, in a discussion of Tatinclaux's [61] paper, presented results for a linear fall-off rate and noted phase shifts in the location of the humps and hollows. Doctors [13] re-examined the hyperbolic distribution in the light of Wilson's criticisms. He claims that the concept should be viewed as, in part, a means of empirically accounting for nonlinearity, surface tension and viscous effects that are otherwise ignored in his model. Doctors further argues that the nature of the fall-off is not important provided comparisons are made on a fair basis.

The shape of the planform can also affect the location and size of the spurious humps and hollows in the wave resistance curve. Newman and Poole [50] noted that the effect is less pronounced for elliptical planforms than for rectangular. It is thought that rounding the corners of the rectangular planform could reduce the size of the spurious behaviour at low Froude numbers. Tatinclaux [61] examined a variety of such pressure field shapes but, as Wilson notes in his discussion of the paper, there are no summary comparisons of the wave resistance of those shapes, so it is difficult to draw any conclusions.

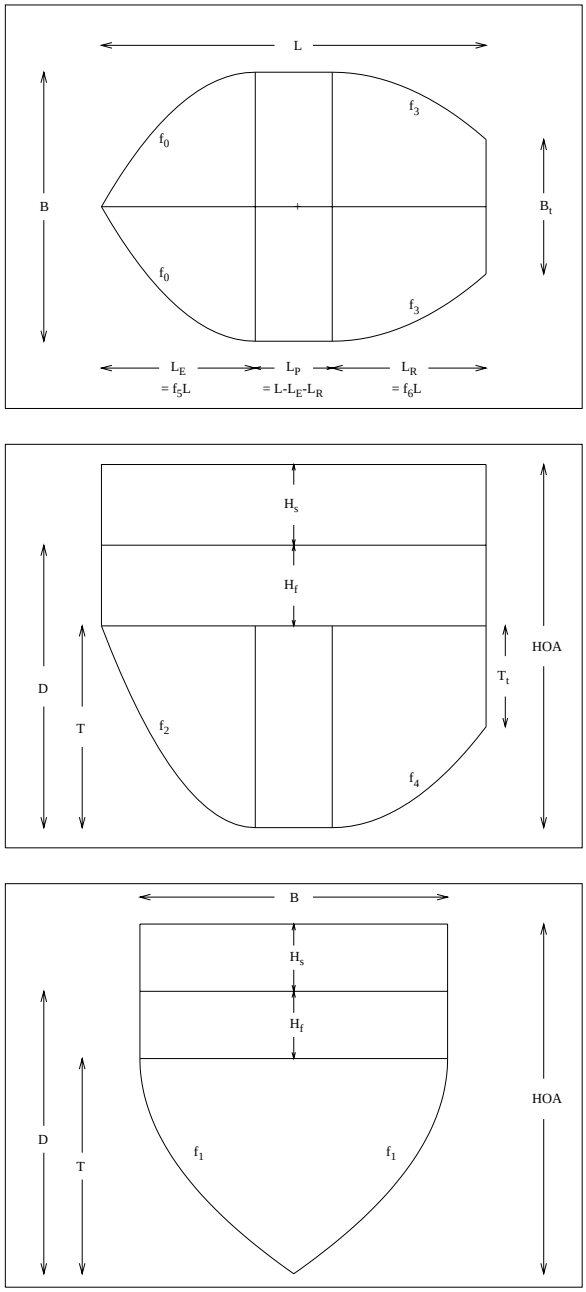

Figure 4: Hull geometry: waterplane (top), sideview (middle) and cross–section (bottom).

2.5 Upright Stability

In a previous optimisation study, Lazauskas and Tuck [39] found that the hulls of vessels optimised for minimum total resistance were often very thin and slender. For monohulls in particular, this represents inadequate upright stability. As a measure of stability we will use the transverse metacentric height, $\overline{GM}_T$, where

$$\overline{GM}_T = \overline{KB} + \overline{BM}_T - \overline{KG}. \tag{2}$$

$\overline{KB}$ is the distance from the keel to the vertical centre of buoyancy:

$$\overline{KB} = \frac{1}{\nabla} \int_{-T}^{0} A_{wp}(z) z dz. \tag{3}$$

$\overline{BM}_T$ is the transverse metacentric radius:

$$\overline{BM}_T = \frac{I_T}{\nabla} \tag{4}$$

where I_T is the (transverse) moment of inertia of the waterplane about the hull's centreline given by

$$I_T = \frac{2}{3} \int_{-L/2}^{L/2} Y^3(x, 0) dx. \tag{5}$$

For a vessel with M hulls, the total transverse moment of inertia is

$$I_{TOA} = \sum_{i=1}^{M} I_{Ti} + A_{wpi}\, w_i^2 \tag{6}$$

where I_{Ti} is the transverse moment of inertia of the i'th hull, and w_i is the lateral distance of the centreline of the i'th hull from the vessel's centreline.

$\overline{KG}$ is the distance from the keel-line to the centre of gravity. At the preliminary ship design stage, $\overline{KG}$ is unknown and must be estimated. In a previous optimisation study of high-speed, multihulled destroyers, Lazauskas [38] used a simple empirical formula to estimate KG on advice from Martin Grimm (pers. comm.) of the Australian Department of Defence. The location of the centre of gravity is assumed to be

$$\overline{KG} = 0.672(\mathrm{TOA} + 0.21\mathrm{LOA}^{0.64}) \tag{7}$$

where TOA is the maximum draft of the vessel and LOA is the overall length of the vessel. The term in brackets is an estimate of the depth, D, of the hull to the main deck and gives very similar results to the depth of so-called "ordinary" ships of "normal form". See, for example, the graphs of Munro-Smith [49] in the U.S. Navy Salvage Engineer's Handbook [56].

For the purposes of the present study we will regard a vessel as unstable if $\overline{GM}_{TOA} < 1.0$m. There are indications that vessels with very large metacentric heights, say $\overline{GM}_{TOA} > 5.0$m, are uncomfortable for crew and passengers, Martin Grimm (pers. comm.).

3 RESISTANCE

Although we are ultimately concerned with the total resistance of high-speed vessels, it is customary to consider the components that make up that total. An (albeit sometimes arbitrary) division into components can give an indication of the relative importance of the physical processes in operation, and this knowledge can be used by naval architects to assess the impact of a variety of design compromises. For example, short stubby vessels have relatively small surface areas and consequently relatively low skin friction. On the other hand, such vessels will, in general, create larger waves and will have a larger wave resistance. If the vessel is to operate in waters where large wave wakes are undesirable then the designer can trade some skin friction for wave resistance by making the vessel more slender in some way.

For the purposes of the present thesis the total resistance, R_T, is considered to be the sum of five non-interacting components, and we write

$$R_T = R_V + R_W + R_A + R_L + R_M \tag{8}$$

where R_V is the viscous resistance, R_W is the wave resistance, and R_A is the aerodynamic resistance on the above-water portion of the vessel. The last two components are applicable only to air-cushion vessels: R_L is the equivalent lift, and R_M is the air-cushion momentum resistance.

We ignore, among other drag components, splash, spray, and wave-breaking which, in general, comprise a smaller proportion of the total resistance than the other components, particularly for the fine slender hulls we shall consider in the present thesis. For SES and ACV we also ignore the drag of the seals containing the air cushion. Unpublished experimental data known to the author indicates that this component is negligible in calm water when there is no contact between the water and the seals.

All computer calculations in the present thesis were performed using the author's computer program `Michlet`. The program has been used by numerous boat-builders and navies for the investigation and design of a wide variety of vessels ranging from small human-powered vessels such as kayaks, rowing shells and solar-powered multihulls [40], to large concept vessels such as the very high speed container vessel investigated by Hearn et al, [34].

The resistance components will now be described in more detail.

Author	Friction Line Formula
Prandtl (1927)	$C_F = 0.074R^{-1/5}$
Telfer (1927)	$C_F = 0.34R^{-1/3} + 0.0012$
Prandtl–Schlichting (1932)	$C_F = 0.455(\log_{10} R)^{-2.58}$
Schoenherr (1932)	$C_F = 0.0586[\log_{10} (RC_F)]^{-2}$
Schultz–Grunow (1940)	$C_F = 0.427(\log_{10} R - 0.407)^{-2.64}$
Kempf-Karman (1951)	$C_F = 0.055R^{-0.182}$
Lap–Troost (1952)	$C_F = 0.0648[\log_{10} (R\sqrt{C_F}) - 0.9526]^{-2}$
Landweber (1953)	$C_F = 0.0816(\log_{10} R - 1.703)^{-2}$
Hughes (1954)	$C_F = 0.067(\log_{10} R - 2)^{-2}$
Wieghardt (1955)	$C_F = 0.52(\log_{10} R)^{-2.685}$
ITTC (1957)	$C_F = 0.075(\log_{10} R - 2)^{-2}$
Gadd (1967)	$C_F = 0.0113(\log_{10} R - 3.7)^{-1.15}$
Granville (1977)	$C_F = 0.0776(\log_{10} R - 1.88)^{-2} + 60R^{-1}$
Date–Turnock (1999)	$C_F = [4.06 \log_{10} (RC_F) - 0.729]^{-2}$

Table 3: Some simple planar friction lines.

3.1 Viscous Resistance

In the present work we assume that a vessel's viscous resistance is due only to the skin friction of the wetted portion of the hulls. The method used for calculating skin-friction is based on von Karman's method as derived and presented by Grigson ([29], [31]). A detailed discussion of Grigson's algorithm is beyond the scope of the present thesis and reference should be made to the cited publications.

The ITTC 1957 line proposed by R.N. Newton (see Grigson [31, p. 81]) at the 1957 Meeting of the International Towing Tank Commission (ITTC) in Madrid is the most popular method in naval architecture for estimating viscous resistance. The line has no basis in physics although it has some peripheral connection to von Karman's theory. The line was adopted as an interim solution because it was the only proposal that seemed to satisfy conference delegates who wanted a friction line that agreed with the Schoenherr line above $R_n = 10^7$, but that was steeper than that line below $R_n = 10^7$, in order to improve correlations for small ship models. Schoenherr's law is

Author	Local Skin-Friction Formula
Prandtl–Schlichting (1932)	$c_f = (2\log_{10} R - 0.65)^{-2.3}$
von Karman (1935)	$\frac{1}{\sqrt{c_f}} = 4.15\log_{10}(Rc_f) + 1.7$
Schultz–Grunow (1940)	$c_f = 0.37(\log_{10} R)^{-2.584}$
Dhawan (1953)	$\frac{1}{\sqrt{c_f}} = 5.06\log_{10}(Rc_f) - 0.91$
ITTC (1957)	$c_f = 0.075(1 - \frac{0.869}{\log_{10} R - 2})(\log_{10} R - 2)^{-2}$

Table 4: Some simple planar local skin friction lines.

empirical, based on data that is spurious, and even the very form of the equation is incorrect. "...this is not Science but guesswork", Grigson [31, p. 113].

In discussions of the ITTC 1957 line, it is common to hear what have almost become mantras...
"The ITTC 1957 line is a model-ship correlation line and not a frictional resistance line." or
"The ITTC 1957 is not a frictional resistance line because it includes a component to account for three-dimensional (or form) effects."

Grigson [29] argues that the distinction between friction line and correlation line is purely semantic, and he further argues that since the 1978 meeting of the ITTC, the line is precisely a friction formula because it is to be used to obtain form factors of single-screw ships, [31, p. 113].

> ...there can be no form factor 'implicit' in the ITTC57 2–D friction line, that would be a contradiction in concept.

Several formulae for estimating the planar drag coefficient C_F are presented in Table 3. This table was compiled from a variety of sources but especially the works by Gadd [26] and Granville [27].

The drag coefficients shown in Table 3 should not be confused with local skin friction coefficients, c_f. The relationship between the two is

$$C_F = \frac{1}{L}\int_0^L c_f dx \tag{9}$$

where L is the total length of the plate.

Table 4 gives several commonly-used formulae for estimating skin friction coefficients c_f.

There is no need to go into the merits and demerits of the various formulae given in Table 3 and Table 4: the important thing to note about these formulae is that both C_F and c_f decrease monotonically and smoothly with increasing Reynolds number. As will be shown later, this type of behaviour is contradicted by accurate experimental evidence.

3.1.1 Outline of numerical method

Author	κ	B_0
von Karman (1934)	0.380	5.50
Prandtl (1935)	0.417	5.80
Clauser (1951)	0.411	4.90
Coles (1954)	0.400	5.50
Smith and Walker (1959)	0.461	7.15
Landweber (1960)	0.420	5.45
Patel (1965)	0.418	5.45
Coles (1968)	0.410	5.00
Winter and Gaudet (1973)	0.384	6.05
Zagarola and Smits (1998)	0.436	6.15

Table 5: Values of the log-law constants κ and B_0 adopted by various authors.

Grigson's method requires the estimation of two constants, κ and B_0, which are usually referred to as the *log-law constants*, and a parameter, Π, called the *wake strength parameter*.

Using values of $\kappa = 0.41$ and $B_0 = 5.0$ Coles fitted several hundred velocity profiles from many different kinds of turbulent boundary layers with very good accuracy [29]. No doubt due to the excellent fit obtained, Coles' values for κ and B_0 are now almost universally accepted.

Recently, Grigson [29] criticised the claim of good accuracy on the grounds that Coles fits were not to measured experiments but to measurements modified to improve the fit. Thus, Grigson [31] argues, it is not independent evidence for the accuracy of the choice of κ and B_0. Other pairs of constants can be found [30] that give fits as good as those using Coles' values.

Grigson claims that Patel's experiments should yield values accurate to ± 1 percent and takes as definitive the values $\kappa = 0.418$ and $B_0 = 5.45$. These values are used in the present work.

Many workers assume a constant value for the wake strength parameter, Π, which is a reasonable assumption for large R_n. Schetz [54, p. 161]) cites a formula due to White for estimating Π as a function of pressure gradient. For a flate plate with zero pressure gradient, White's formula reduces to

Author	Π
Coles (1968)	0.55
Wieghardt (1968)	0.59
Model of R. Michel (1968)	0.38
$k-\epsilon$ model (1972)	0.29
White (1974)	0.476
Model by Cebeci and Smith (1974)	0.55
Grigson (1989)	0.45
Grigson (2000)	0.437

Table 6: Large Reynolds number limit for the wake strength proposed by various authors.

$\Pi = 0.476$. Several other estimates for the large R_n limit of Π are tabulated in Schlichting [55, p. 583] and are included in Table 6.

Using the experimental data of Smith and Walker [60], Grigson [30] calculated the large R_n limit of the wake strength parameter to be $\Pi = 0.45$. He also suggested that a 5% error in the determination of Π causes an error of about 1/2 % in the planar drag coefficient C_F. In a later work, Grigson [31] included additional experimental data into his analysis and revised the large R_n limit to $\Pi = 0.437$.

For small R_n, the value of Π varies in a manner that can be determined from experiment, however Grigson [31] warns that the determination from measured velocity profiles is very difficult for $R_2 < 3000$, where R_2 is boundary layer momentum thickness.

The behaviour of Π as a function of boundary layer momentum thickness is shown in Figure 5. The curves for the present algorithm and Grigson's cubic spline fit to data from several sources are identical for $\log_{10} R_2 > 4.0$. For $\log_{10} R_2 < 4.0$ the curve for the present model was constructed to ensure a better fit to Dhawan's [11] experimental local skin friction coefficients at low R_n. The curve for Cebeci and Smith's equation was taken from the graph in Grigson [29, Fig. 4, p. 152].

It must be emphasised that for large R_n, i.e. at ship-scale, the low-R_n behaviour of Π becomes insignificant in the calculation of skin friction coefficients.

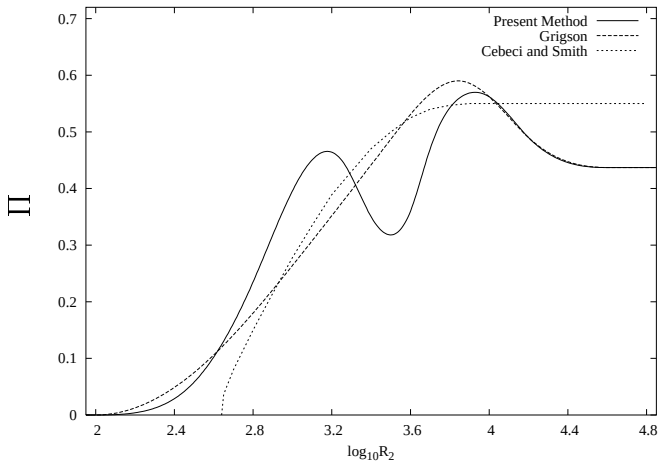

Figure 5: Wake strength parameter as a function of boundary layer momentum thickness Reynolds number.

3.1.2 Verification of friction resistance predictions

Figure 6 compares planar drag coefficients predicted by four methods. For $R_n < 10^6$, the present method predicts values for C_F that are significantly smaller than the other methods. There is a noticeable bulge in the curve for the present method for $10^6 < R_n < 10^{6.5}$ which is a direct consequence of the low R_2 behaviour of the wake shape parameter, Π. Results calculated with the present algorithm are almost identical to Grigson's for $R_n > 10^7$ and his curve has been omitted from the bottom half of the figure. Predictions for the three methods shown in the bottom of Figure 6 are very close for $R_n \approx 10^{7.1}$. For $R_n > 10^{7.1}$ the present method predicts values of C_F that are greater than both the ITTC 1957 line and the method of Prandtl-Schlichting.

Figure 7 shows predictions of C_F using the same methods as in Figure 6 but here given as a ratio of the C_F predicted by the present method. It can be seen that the difference between the present method and the Prandtl-Schlichting line is no greater than 5% for the entire range of R_n shown in the figure. For $10^6 < R_n < 10^7$, i.e. at small ship model scale, the predictions of the present method are about 5% less than those predicted by the ITTC line. For $R_n \approx 10^9$, i.e. for full-scale high-speed ships, the present method predictions are about 5% higher than those of the ITTC line.

Figure 8 compares the local skin friction, c_f, from Smith and Walker's experiments with several skin friction formulae. Both their velocity profile

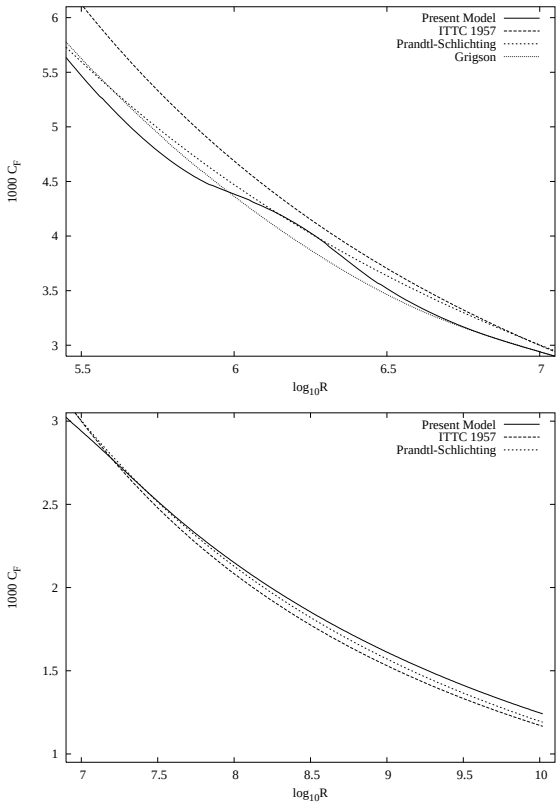

Figure 6: Comparison of planar drag coefficient predictions at low R_n (top) and high R_n (bottom).

data and their balance data are shown in the figure.

There is very little reliable experimental data for c_f at low R_n. Dhawan's [11] experiments at NASA with both laminar and turbulent boundary layers are a useful resource, but the scale of Dhawan's graphs makes it difficult to read off individual points. Instead of attempting to reproduce Dhawan's data points we have simply plotted six points in the top graph of the figure using the formula given in Table 4 that Dhawan fitted to his own experimental data.

It can be seen that, apart from the present method, the simple formulae over-predict c_f for $R_n < 10^{6.1}$. Grigson's method over-predicts Dhawan's experiments and tends to under-predict Smith and Walker experiments. That the present method follows Dhawan's results accurately and then changes

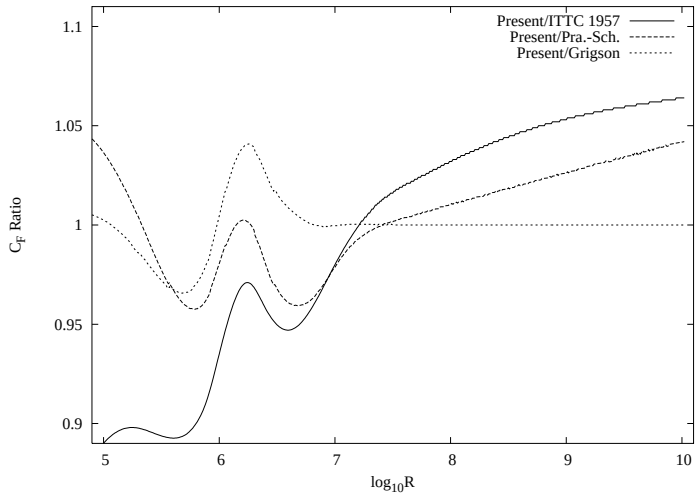

Figure 7: Ratio of planar drag coefficients predicted by the present method and by using some commonly–used formulae.

slope in the range $10^{5.8} < R_n < 10^{6.2}$ is due solely to the form chosen for the wake strength parameter Π. For $R_n > 10^7$ the present method and Grigson's original algorithm are almost identical.

Figure 9 shows predictions of c_f for $R_n > 7.5$ using the present method, the ITTC line and the Prandtl-Schlicting formula. The curve for the present method is close to the curve calculated using the Prandtl-Schlichting formula; slightly less than the formula for $R_n < 10^{8.25}$, and slightly greater for $R_n > 10^{8.25}$. The present method and Prandtl-Schlichting predict values of c_f that are about 6% higher than the ITTC line for the entire range of R_n shown in the figure.

In the present work we will not employ additional form factors. Grigson [31], attempted to extend his method to include form factors so that estimates of the viscous resistance could be made with confidence, rather than just the skin friction. In this regard his efforts were, on the whole, unconvincing. It should be noted however, that he himself introduced the section on form factors with the words, [31, p. 97], "This part of the work is wholly empirical, pure concoction."

In 1999, the 22nd ITTC Committee [52] repeated their long-standing recommendation that no corrections for form effects be made in routine predictions of high speed marine vehicles.

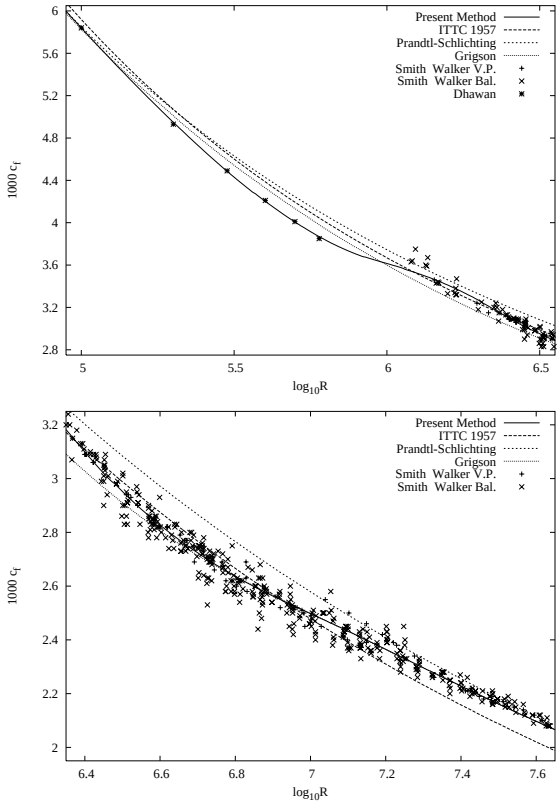

Figure 8: Estimated local skin friction coefficients at low R_n compared to the experiments of Dhawan and of Smith and Walker.

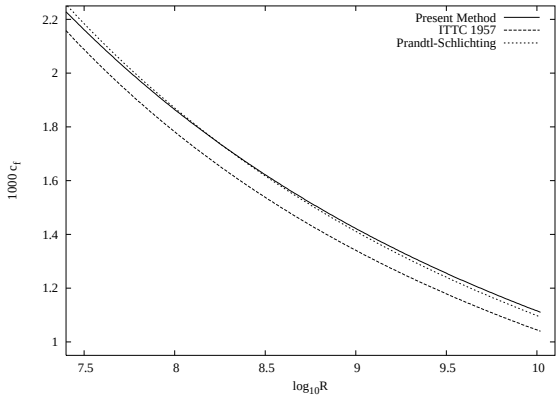

Figure 9: Estimated local skin friction coefficients at high R_n.

3.2 Wave Resistance

The wave-making problem is here formulated under the assumptions that the fluid is homogenous, inviscid and incompressible (and hence moves irrotationally), and that surface tension effects can be neglected. We also assume that the water is infinitely deep and laterally unbounded. These (ideal) conditions reduce the task from one of solving the full Navier-Stokes equations to the much simpler (but still challenging) problem of solving Laplace's equation

$$\phi_{xx} + \phi_{yy} + \phi_{zz} = 0 \tag{10}$$

for the disturbance velocity potential $\phi(x, y, z)$ to a uniform, steady stream U due to the presence of an assembly of bodies close to the free surface $z = Z(x, y)$.

3.2.1 Free-wave spectrum

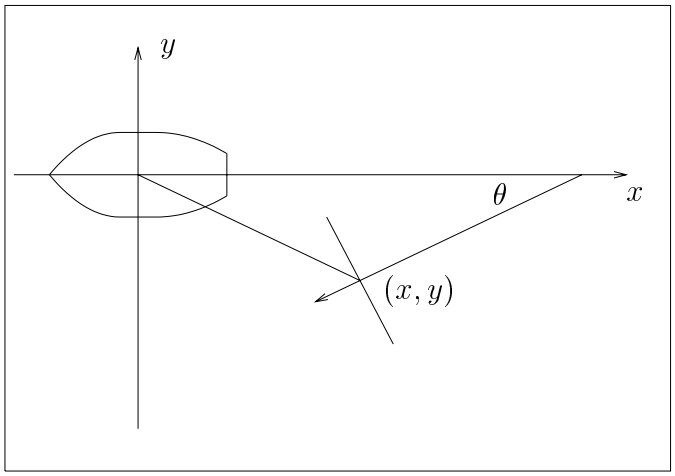

Figure 10: Coordinate system. θ is the angle of propagation (positive to port) of the wavefront passing through the point (x, y).

Under the simplifying assumptions given above, the steady wave pattern $z = \zeta(x, y)$ of any ship, as seen at a point (x, y) sufficiently far behind the ship, can be considered as the sum of plane waves travelling at various angles θ of propagation relative to the direction of motion of the ship. See Figure 10.

According to Havelock [33], Tuck et al [64],

$$\zeta(x,y) = \Re \int_{-\pi/2}^{\pi/2} A(\theta)\, e^{-ik(\theta)\,\omega(x,y,\theta)} d\theta \tag{11}$$

where $A(\theta)$ is the (complex) amplitude function, sometimes also called the free wave spectrum or Kochin function; $k(\theta)$ is the wave number of the waves travelling at angle θ, and ω is a phase function with

$$\omega(x,y,\theta) = x\cos\theta + y\sin\theta. \tag{12}$$

In the present work, we assume infinite depth water. The appropriate wave number is then given by

$$k(\theta) = k_0 \sec^2\theta \tag{13}$$

where $k_0 = g/U^2$, g is the acceleration due to gravity, and U is the ship speed. Note that the contributions to the integral in equation (11) from *positive* angles θ correspond to waves being propagated to the *left* or *portside* of the vessel. Once $A(\theta)$ has been specified for a given form of the dispersion relation (here equation (13)), it can be used to determine the actual wave pattern, and also the total energy of that wave pattern, and hence the wave resistance

$$R_W = \frac{\pi}{2}\rho U^2 \int_{-\pi/2}^{\pi/2} |A(\theta)|^2 \cos^3\theta\, d\theta. \tag{14}$$

We now assume that the wave field created by a combination of hulls and pressure distributions can be constructed by linear superposition of wave fields generated by amplitude functions for each hull and each pressure distribution, each acting independently of the other disturbances. Hydrodynamic interactions between disturbances, other than wave intereference effects, are assumed to be negligible. The case without pressure distributions was investigated in Tuck and Lazauskas [70].

Suppose that there are M such disturbances due to displacement hulls, and N disturbances due to pressure distributions. The disturbances can be located anywhere in the xy-plane. Furthermore, suppose that the displacement hull numbered m located at (x_m, y_m) has amplitude $A_{H_m}(\theta)$ and that the pressure distribution numbered n located at (x_n, y_n) has amplitude $A_{Pn}(\theta)$. The total far-field wave is then

$$\zeta(x,y) = \Re \int_{-\pi/2}^{\pi/2} d\theta\, e^{-ik\omega} \left\{ \sum_{m=1}^{M} A_{H_m}(\theta)\, e^{ik\omega_m} + \sum_{n=1}^{N} A_{P_n}(\theta)\, e^{ik\omega_n} \right\} \tag{15}$$

where $k = k(\theta)$, $\omega_m = x_m \cos\theta + y_m \sin\theta$, and $\omega_n = x_n \cos\theta + y_n \sin\theta$.

That is, the general expression (11) still applies to the whole vessel, with

$$A(\theta) = \sum_{m=1}^{M} A_{H_m}(\theta)\, e^{ik\omega_m} + \sum_{n=1}^{N} A_{P_n}(\theta)\, e^{ik\omega_n} \tag{16}$$

The complex amplitude can be computed by various means, Tuck and Lazauskas [70], e.g. a complete nonlinear near-field computation, by experimental measurement or by approximations such as small disturbance theory. For the wave field induced by displacement hulls we will employ the small disturbance theory of Michell [47]. This approximation allows us to write the amplitude function as

$$A_{H_m}(\theta) = \frac{-2ik^2}{\pi} \int\!\!\int_{R_m} Y(x,z)\, \exp\left(kz + ikx\cos\theta\right) dxdz \tag{17}$$

where the offsets of the hull are $\pm Y_m(x,z)$ relative to the (vertical) centreplane, R_m, of the m-th hull .

A similar theory to Michell's can also be used for pressure distributions, see for example Doctors [13]. The complex amplitude for these disturbances can be written as

$$A_{P_n}(\theta) = \frac{k^2}{\pi\rho g} \int\!\!\int_{B_n} p(x,y)\, \exp\left(ik\omega\right) dxdy \tag{18}$$

where $p_n(x,y)$ is the pressure distribution acting over the region B_n of the xy-plane.

3.2.2 Method of calculation

The integrands of the complex amplitude functions given by equations (17) and (18) are highly oscillatory, and special techniques are required for the evaluation of the integrals. Tuck [65], Tuck and Lazauskas [71], and Tuck, Scullen and Lazauskas [73] have developed efficient computer routines for the evaluation of the integrals. These routines use Filon's quadrature [25] to capture the rapid oscillations as $|\theta| \to \pi/2$. Conventional, (e.g. Simpson) quadratures fail to capture the correct decay of the spectrum in this region, Tuck, Scullen and Lazauskas [79].

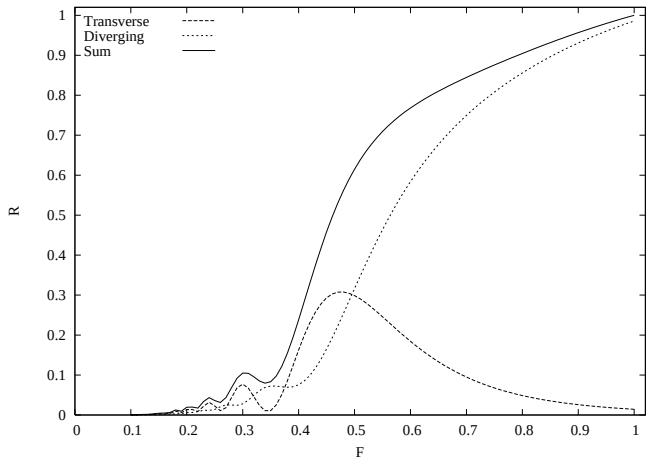

Figure 11: Wave resistance components of standard Wigley hull.

3.2.3 Transverse and diverging wave systems

Figure 11 shows the wave resistance of a standard Wigley hull. It also shows the proportions of the total wave resistance due to transverse waves ($0 \leq \theta \leq \arcsin(1/\sqrt{3}) = 35.3°$), and diverging waves ($\theta > 35.3°$).

Clearly, if we wish to reduce the wave resistance of this ship for a specific Froude number, we should choose a method of wave cancellation that is appropriate to that Froude number. For vessels operating at Froude numbers greater than about 0.5 it is important to concentrate efforts on the diverging wave system. This general theme was examined in detail by Tuck and Lazauskas [70].

Figure 12 shows the free wave spectrum for the same hull at three Froude numbers. (The wave resistance R_W is proportional to the area under the curve.) It can be seen that the angles at which the maximum energy is propagated varies with Froude number. For the lowest Froude number, $F = 0.418$, most energy is shed for the range $0 \leq \theta < 35°$, which corresponds to the transverse wave system. If it is not possible to reduce transverse waves for one reason or another, it might be profitable to try cancelling waves at $\theta \approx 60°$ where there is a smaller hump in the free wave spectrum curve. For the higher Froude numbers, the maximum in the curves appears at higher θ. The energy shed in the form of transverse waves is much less than at low F and, in general, there is one dominant peak in the curves where we should, if possible, concentrate any wave cancellation methods at our disposal.

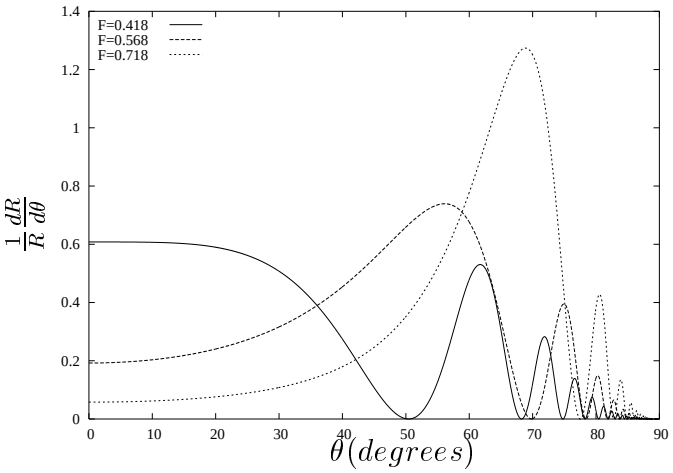

Figure 12: Non-dimensional free wave spectrum of standard Wigley hull at three Froude numbers.

Figure 13 shows the angle at which peaks and hollows occur in the free wave spectrum of the same Wigley hull. Also shown are the curves of rational polynomials fitted to the points predicted by the theory. These approximations can be useful design formulae to quickly estimate the location of the peaks and hollows. The approximating functions are given by

$$\theta(F) = A\frac{(F-B)(F-C)}{(F-D)(F-E)} \tag{19}$$

where θ is the wave propagation at which a peak (or hollow) occurs, F is the Froude number, and A, B, C, D, and E are constants chosen so as to minimise the square of the differences between the approximation and values calculated using the present numerical method. The constants used in the approximation formulae are given in Table 7.

Free wave spectra for travelling pressure distributions have the same overall appearance as those for displacement vessels. For example, see Tuck, Scullen and Lazauskas [79, p. 12] for free wave spectrum plots of a variety of pressure distribution arrangements.

3.2.4 Wave interference and cancellation

Figure 14 shows the catamaran width-to-length ratio required to eliminate waves propagating at the angle at which the first peak occurs in the free

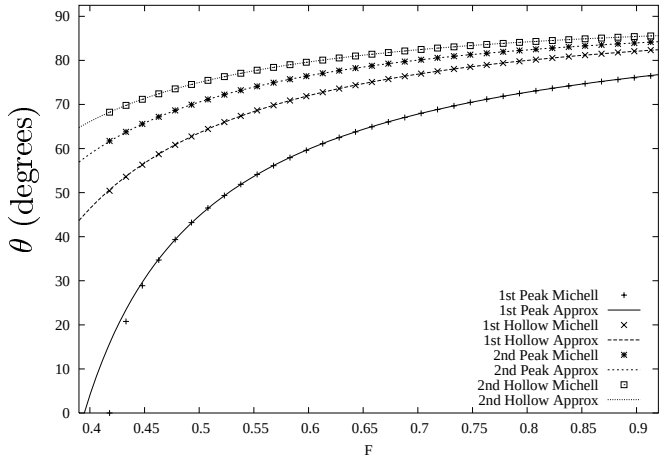

Figure 13: Angle at which peaks and hollows occur in the free wave spectrum of a standard Wigley hull. Points were calculated using the present theory; curves are rational polynomials fitted to those points.

	A	B	C	D	E
1st Peak	0.4613	8625.9023	0.3949	43.6704	0.2834
1st Hollow	-0.2041	0.3048	9337.7020	0.1953	-18.7080
2nd Peak	-0.3935	0.2690	9018.6251	0.1850	-36.3864
2nd Hollow	-0.2986	0.2395	8945.4573	0.1651	-27.2004

Table 7: Coefficients of rational polynomials.

wave spectrum of a standard Wigley monohull. The catamaran comprises two Wigley demihulls, each with the same length and draft as the equivalent monohull, but half the displacement (and therefore half the beam) of the monohull. The two curves in the graph are approximations fitted to the points. The curve labelled "Rational Linear" is given by

$$\frac{w}{L} = \frac{0.0814}{(F - 0.3545)} \tag{20}$$

and the curve labelled "Rational Quadratic" is given by

$$\frac{w}{L} = -15.4754 \frac{(F + 0.2580)(F - 1.9538)}{(F - 0.3728)(F + 238.9930)} \tag{21}$$

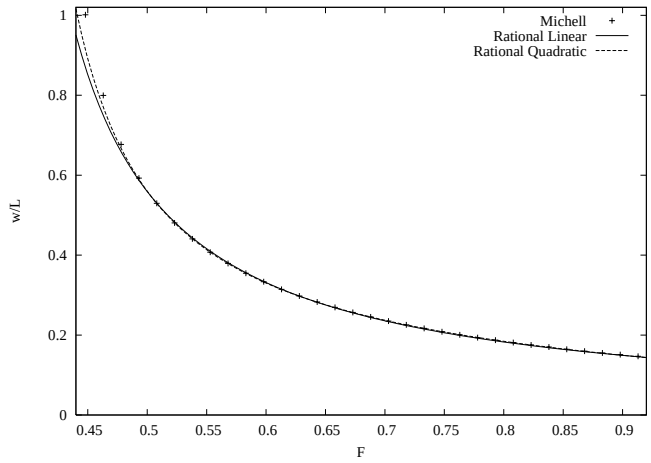

Figure 14: Catamaran width-to-length ratio required to eliminate waves propagating at the angle at which the first peak occurs in the free wave spectrum for a standard Wigley monohull.

The results shown in Figure 14 are an extension of the work by Tuck and Lazauskas [70] on the optimal spacing of catamarans. There, [70] p. 188, we determined the optimum lateral separation required to eliminate waves propagating at a given angle θ. Here, we have assumed that the objective is to eliminate waves propagating at the first peak in the free-wave spectrum of the equivalent monohull for a given Froude number. If we assume a practical lateral separation range of $0.2 < w/L < 0.33$, it is clear from Figure 14 that there is only a relatively narrow band of Froude numbers (about $0.6 < F < 0.77$) for which we can eliminate waves at the first peak in the free wave spectrum.

The approximation formulae may find some use in preliminary design work, but only for the range of Froude numbers shown in Figure 14. While strictly applicable only to Wigley hulls, the curves should be reasonably accurate for other hulls with roughly parabolic waterlines.

In his work on the wave resistance of SES, Yim [84] analysed the wave resistance of several combinations of pressure planforms, side wall displacements, and the effect of front and rear skis. He concluded [84, p. 32] that future investigations should include fore–aft asymmetry of pressure planform and side hulls, the effect of vortex shedding from side hulls, and the effect of wave reflections between side hulls. The insights that can be gained by a

close examination of the free wave spectrum for monohulls and catamarans suggests that similar insights might be gained for SES. For example, it might be possible, by a judicious choice of hull shapes and pressure variations, to effect some beneficial wave cancellation, and the free wave spectra of the hulls and pressure distributions could give valuable clues.

There are also indications that lateral asymmetry of the demihulls can reduce the wave resistance of catamarans. In a very recent work, Tuck [67] has shown that the possible reduction is significant only when the demihull spacing is suboptimal. When demihulls are spaced optimally, there is little opportunity for wave resistance reduction by cambering the side hulls. In the present work we will consider only laterally symmetric demihulls.

3.3 Air Resistance

Air resistance is estimated in the manner suggested by Day et al [9].

$$R_A = \frac{1}{2} C_D \rho U^2 A_f \tag{22}$$

where it is assumed that the value of the (bluff body) drag coefficient is $C_D = 0.4$.

For the vessels to be considered later in this thesis, the frontal area, A_f of the above-water portion of a monohull, multihull and ACV, is assumed to be

$$A_f = B_{max} H_a \tag{23}$$

where B_{max} is the maximum beam of the vessel, and where H_a is the above-water height.

The way in which the space inside the vessel is arranged into deck, cargo holds, etc will, of course, be largely determined by the mission. For their catamarans, which are somewhat larger than we will consider, Day et al, [9] assume a constant above-water height of 15.5m. Their assumed value is based on a tunnel clearance of 3.5m, a 1.5m deep cross-structure atop which rests an 8.0m cargo space and a 2.5m passenger deck. In the present thesis, we assume that $H_a = 16.0$m for all vessels.

For SES, when the vessel is fully supported by the hulls (i.e. $\sigma = 1$, $\tau = 0$), we assume the same frontal area as for the other vessels. When partly-supported by the air cushion (i.e. $\sigma < 1$, $\tau > 0$), the sidehulls are lifted out of the water with an attendant increase in the above-water frontal area.

As will be seen later, wide vessels at high speeds can have significant air resistance. A rough estimate using the approach described above may be satisfactory for preliminary design purposes, but eventually more refined estimates will be required.

It should be noted that for military applications, large above-water structures are undesirable because of issues to do with visibility and stealth. Many modern naval designs have a low profile with hull panels angled in a way to reduce their visibility to radar. The low profile will reduce the frontal area and hence the air resistance; however the angled panels will increase the drag coefficient.

3.4 Air-cushion Momentum Resistance

According to Day et al [9], air escaping from under the skirt of an ACV transfers momentum from the vessel to the air which means that a force acts on the vessel. This "momentum air resistance" is given by

$$R_M = \rho_{air}\, Q_c\, U \tag{24}$$

where ρ_a is the density of air, and Q_c is the volume flow rate of air escaping from the cushion, assumed for purposes of calculation to be at uniform pressure p_c, the mean cushion pressure.

Q_c can be estimated as

$$Q_c = L_p\; h_c\; q\; C_q \tag{25}$$

where L_p is the perimeter of the skirt (equal to twice the tunnel width for a SES, or twice the sum of length and tunnel width for an ACV). h_c is the (nominal) distance between the water surface and the bottom of the skirt, here assumed as in [9] to be 0.1m. The coefficient C_q accounts for the contraction of the escaping air jet. We follow [9] and use $C_q = 0.6$.

The velocity of air escaping between the water surface and the skirt, q, can be calculated using Bernoulli's equation

$$q = \sqrt{2p_c/\rho_a} \tag{26}$$

A more thorough examination of this problem can be found in, among others, Jones [35] and Tselnik [63].

3.5 Equivalent Lift

Inflating and sustaining an air cushion requires power. Although the power required is independent of speed, for the purposes of comparing resistance components we follow Day et al [9] and define an equivalent lift resistance

$$R_L = (\eta_T/\eta_L)(p_c\, Q_c/U) \tag{27}$$

where η_T is the thrust efficiency and η_L is the lift efficiency. We also assume, as in [9], a value of 2.0 for the ratio η_T/η_L, claiming that it will adequately account for, among other factors, losses in air intake and ducting.

3.6 Verification of Resistance Predictions

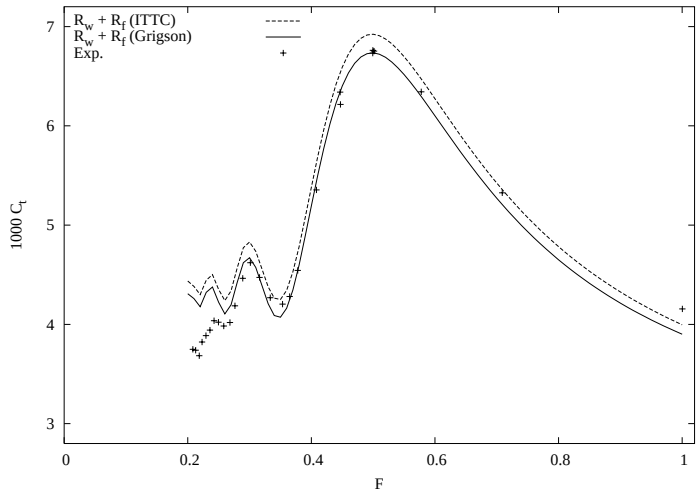

Figure 15: Comparison of experimental total hydrodynamic resistance coefficients for a parabolic strut with two methods of estimating skin friction.

Day et al [8] devoted almost their entire paper to the investigation of the resistance predictions made by Tuck and Lazauskas [70] for some conventional and for some unconventional multihull arrangements. Although the demihulls used in their numerical and their experimental work were not identical to those used in [70], Day at al [8] concluded that wave resistance could be reduced substantially by employing longitudinally staggered hulls in the manner we suggested. They also concluded that the resistance of the vessels could be predicted with "reasonable accuracy" using thin-ship theory.

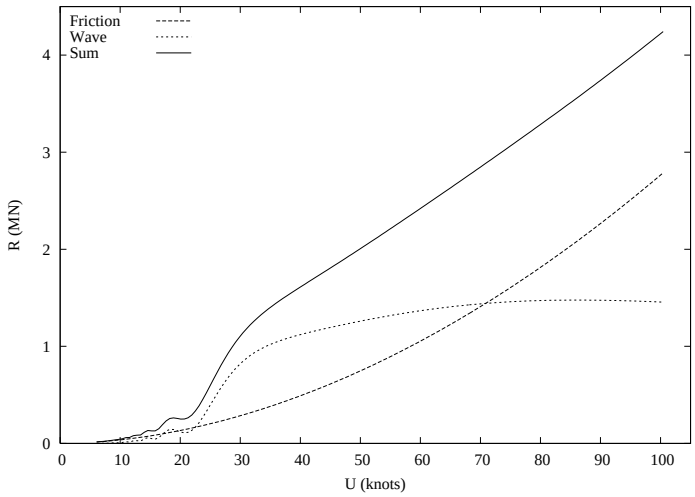

Figure 16: Hydrodynamic resistance components (in Mega Newtons) of a 100m standard Wigley hull.

Figure 15 compares Sharma's [58] experimental measurements of the total resistance (here defined as $R_T = R_F + R_W$) of a thin parabolic strut ($L/B = 20.0$) with predictions, using two different methods for estimating the skin–friction. For Froude numbers below about 0.6, our extension of Grigson's method gives, in general, better agreement with experiments. For Froude numbers greater than 0.6, the ITTC line is superior.

Figure 16 shows the predicted frictional and wave resistance components (in mega Newtons) of a 100m long, standard Wigley hull using the method of the present work, i.e. Grigson's method for the skin–friction, and Michell's thin-ship theory for the wave resistance.

Table 8 shows some Froude numbers at which interesting features occur in the resistance curves or the free wave spectrum curves of the ship. See also Figure 12 and Figure 11.

F	U (ms^{-1})	U $(knots)$	Comments
0.3220	10.09	19.60	$R_f \approx R_w$
0.3414	10.69	20.78	Hollow in R_w curve
0.3449	10.69	20.99	Hollow in R_{wt} curve
0.3545	11.10	21.58	Hump in R_{wd} curve
0.3691	11.56	22.47	Hollow at Kelvin angle in FWS
0.3696	11.58	22.50	$R_f \approx R_w$
0.3756	11.76	22.86	$R_{wt} = R_{wd}$
0.3809	11.93	23.19	Hollow in R_{wd} curve
0.3989	12.49	24.28	$F = 1/\sqrt{2\pi}$: bow and stern waves cancel
0.4646	14.55	28.28	Peak at Kelvin angle in free wave spectrum
0.4761	14.91	28.98	Maximum R_{wt}
0.4954	15.51	30.16	$R_{wt} = R_{wd}$
0.5642	17.68	34.34	$F = 1/\sqrt{\pi}$: bow and stern waves reinforce
1.0000	31.32	60.87	Speeds corresponding to $F = 1$
1.1640	36.45	70.85	$R_f \approx R_w$
1.4172	44.38	86.27	Maximum R_w
1.4332	44.88	87.24	Maximum R_{wd}
1.6428	51.44	100.00	Froude number corresponding to 100 knots

Table 8: "Interesting" Froude numbers for a 100m standard Wigley hull. R_{wt} is the wave resistance due to transverse waves; R_{wd} is the resistance due to the diverging wave system.

4 EFFECT OF PARAMETRIC VARIATIONS

There are two main ship design processes. "Point-based" design emphasises the interaction of many design components such as resistance, weight, volume, stability etc, and considers each in turn, Parsons [51]. The "design spiral" is a traditional pictorial representation of the iterative process, Eames and Drummond, [21]. In general, the objective is to find a single design that satisfies the requirements of the mission and other, (e.g. safety,) constraints. The main disadvantage of the point-based design process is that feasible designs may not be globally optimal in terms of some given measure of merit, [51].

In contrast to point-based design, "set-based" approaches begin from a broad set of design parameters and retain the breadth of possibilities until specific design decisions have to be made; the so-called "Principle of Least Commitment", [51]. The constraint sets are, as with point-based design, ultimately narrowed down to a single solution, but the hope is that a more global optimum will have been found than if constraints were narrowed earlier in the process.

Regardless of the design approach, it is clear that specifying constraints is important. Unfortunately, only experience can guide us in setting the range of a given geometric parameter. We will rarely know in advance whether the range allowed for a given parameter is too narrow (so that a good solution will be missed) or too broad so that much effort will be wasted on infeasible or impractical solutions.

4.1 Hull Shape

Name	f_1	f_2	B	$\overline{GM}_T$
Strut	0.0	0.0	7.59	-1.74
Spheroid	0.5	0.5	10.93	0.73
Canoe	1.0	1.0	14.22	4.74
Wigley	1.0	0.0	11.38	1.16

Table 9: Effect of hull shape on the beam and upright stability of four 1200 tonne monohulls with length 76.41m and draft 3.106m.

Suppose that our task is to design a monohull vessel of total displacement 1200 tonnes, length 76.41m, and draft 3.106m. To reduce the number of shape parameters for pure displacement vessels we will only consider hulls with parabolic waterlines, i.e. $f_0 = 1$ in the hullform series described earlier. Furthermore, we will restrict our attention to fore-aft symmetric hulls that have no parallel middlebody and that do not have a transom stern. From the eight parameters available in the series described earlier, we now have freedom only to choose the cross-section shape, f_1, and the keel-line shape, f_2.

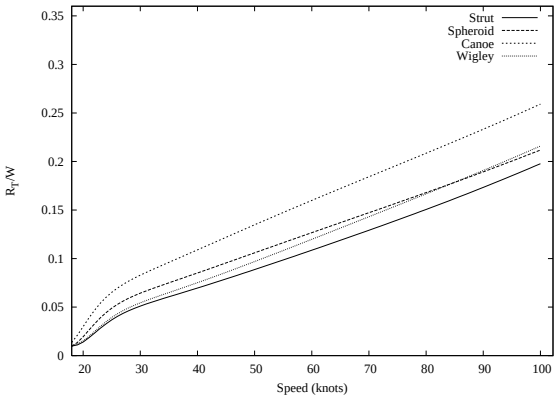

Figure 17: Effect of hull shape on the specific resistance of four 1200 tonne monohulls with length 76.41m and draft 3.106m.

Table 9 shows the beam, B, and the transverse metacentric height, $\overline{GM}_T$, of four hulls with different pairs of shape parameters, f_1 and f_2. (The names of the four hulls will be used in the discussion when they are more suggestive than the shape parameter values.) Figure 17 shows the specific resistance, R_T/W, for these hulls as a function of speed in knots.

Strut has the smallest beam of the four examples, and the lowest total resistance, but it is also unstable according to the criterion we specified earlier, i.e. $\overline{GM}_T < 1$. *Spheroid*, the hull with elliptical cross-sections and an elliptical keel-line, has a wider beam than *Strut* but, with $\overline{GM}_T = 0.73$, it is also unstable. *Canoe* has parabolic cross-sections and parabolic sideview. It has the widest beam of the four hulls and is stable according to our criterion, but it also has the largest total resistance for the entire range of speeds shown in Figure 17. The beam of the Wigley hull is similar to that of *Spheroid*, but it is stable, since $\overline{GM}_T = 1.16$m.

If our choice was limited to the four hulls given in Table 9, the Wigley hull would be a clear winner: *Strut* and *Spheroid* are unstable, and *Canoe* has much higher total resistance.

This very simple example shows that it may sometimes be unwise to limit the range of shape parameters too severely, particularly if we are not doing so for practical engineering reasons. If, for example, we had specified that $0.5 \leq f_2 \leq 1.0$, in the hope that it would speed up the search for an optimum, we would have excluded *Strut* and *Wigley* hull from consideration, thereby missing the best vessel.

4.2 Demihull Separation

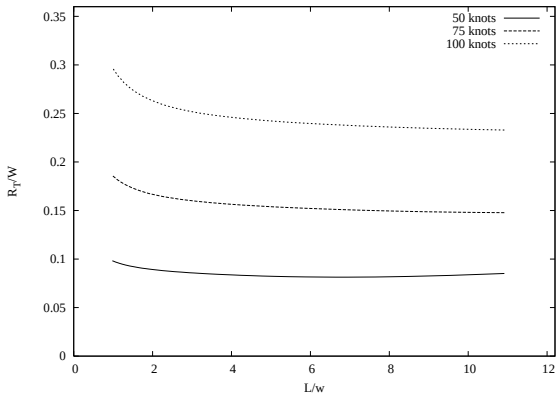

Figure 18: Effect of demihull lateral separation on the specific resistance of a 76.41m, 1200 tonne catamaran at three design speeds.

Figure 18 shows the specific resistance of a 76.41m, 1200 tonne catamaran as a function of length-to-width ratio for three design speeds, namely 50, 75, and 100 knots. The length-to-width ratio is L/w where L is the demihull length and w is the transverse distance between the centrelines of the demihulls. The demihulls are identical to the *Wigley* hull in the previous section. Here, however, they each have half the displacement of the monohull and, since length and draft are the same as before, they therefore each have half the beam of the monohull. Since wave resistance varies as the square of the beam, each demihull has one quarter of the wave resistance of the equivalent monohull.

At 50 knots, the Froude number of this 76.41m vessel is about 0.94. We can estimate the optimum demihull separation distance by assuming that it is the distance required to eliminate waves propagating at the first peak in the free wave spectrum of the Wigley hull. Using $F = 0.94$ in equation (20), we estimate the optimum lateral separation as $w/L = 0.14$ or, in terms of the horizontal scale of Figure 18, its reciprocal, $L/w = 7.1$. Viscous resistance is constant for all demihull separation distances.

For the higher design speeds, 75 knots and 100 knots, the optimum lateral separation will be much less than 0.14, which is already very narrow when compared to most existing catamarans. The INCAT86 built by International Catamarans Pty Ltd has a similar displacement and length to our example, and it has $w/L \approx 0.284$, i.e. about twice the width.

The effect of demihull lateral separation distance on the three resistance components (i.e. viscous, wave and air) is shown in Figure 19. Air resistance is shown with a different scale to the other two plots in the interests of clarity.

Viscous resistance is a (different) constant for each design speed, and comprises the most significant proportion of the total resistance. Wave resistance becomes less important as the design speed increases. At 50 knots, it comprises between about 30% and 40% of the total resistance; at 100 knots, it is responsible for about 15%. As expected, air resistance becomes significant for the wider vessels at high speed.

If the objective is to minimise total resistance then, in general, it seems sensible to focus attention on the largest contributor to the total, in this case the viscous resistance. But there is clearly nothing to be gained here by choosing the demihull spacing: a judicious choice of demihull separation will serve only to reduce the air resistance and to possibly reduce the wave resistance.

In practical terms, employing the optimum lateral separation distance in order to reduce total resistance at high speed will require a very significant reduction in deck area. In fact, the optimum spacing might not be achievable at all if the beam of the demihulls cannot be less than some minimum determined from structural considerations.

In the previous example we saw that it can sometimes be imprudent to constrain too tightly the range of parameters in case we miss an optimal solution. The present example illustrates the situation where we may have to completely ignore the direction in which analysis points us, and apply some other criteria to constrain the geometry of candidate vessels.

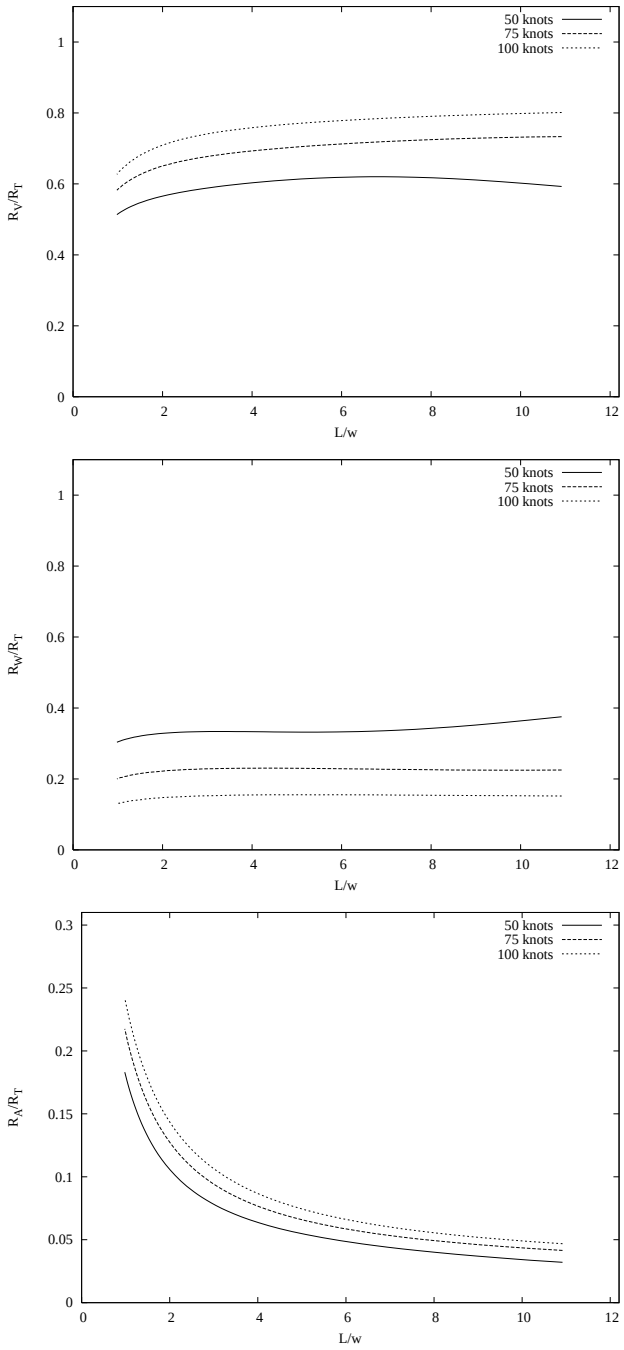

Figure 19: Effect of demihull lateral separation on the viscous resistance fraction (top), wave resistance fraction (middle) and air resistance fraction (bottom) of a 76.41m, 1200 tonne catamaran at three design speeds.

4.3 Pressure Patch Width

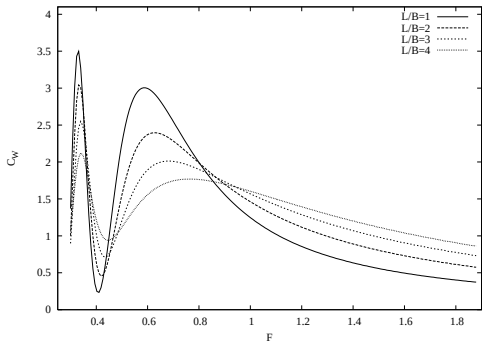

Figure 20: (Newman-Poole) wave resistance coefficient as a function of length-based Froude number for 1200 tonne ACV of varying length-to-beam ratios.

For an ACV comprising a rectangular constant pressure patch of fixed length and displacement, the only freedom we have is to vary the width of the patch. Of course by varying the width only, we are in effect choosing the mean pressure.

Figure 20 shows the (Newman-Poole) wave resistance coefficient, C_{np}, as a function of length-based Froude number for four pressure distributions of varying width. The wave resistance coefficient is defined as

$$C_{np} = \frac{\rho U^2 \kappa^2}{p_0^2} R_W \tag{28}$$

where U is the speed, $\kappa = g/U^2$, p_0 is the mean pressure, and R_W is the wave resistance.

If we fix the length of the pressure distribution at 76.41m, the same as in the previous examples, then the Froude number at 50 knots is about 0.94; at 75 knots, $F = 1.41$; and at 100 knots, $F = 1.88$. The most noticable features of the graph are prominent humps in the curves at about $F = 0.3$ and $F = 0.6$, however these correspond to speeds well below our region of interest, as does the prominent hollow in the curve at about $F = 0.4$. For $F > 0.9$ there are clear trends for C_{np} with both L/B and F: wave resistance is lower for wider vessels. If our objective was low wave resistance then we could simply aim for the widest vessel practical considerations will allow.

The top graph of Figure 21 shows the specific resistance for the four ACV over a wide range of speeds; the bottom graph shows the effect of width on

the specific resistance for three design speeds. The top graph shows that the widest (here $L/B = 1$) vessel is a good choice for speeds up to about 67 knots. At higher speeds, narrower vessels are better.

The bottom figure shows that there are minima in the curves for each of the three design speeds: for 50 knots, the optimum is at about $L/B = 0.94$, at 75 knots $L/B \approx 1.6$, and at 100 knots $L/B \approx 2.3$. These optimal ratios correspond to widths that are very much larger than the optimum demihull spacing of the catamarans in the previous example. Thus, for SES, (ignoring the effect of wave interference for a moment), we expect that there will be opposing trends with regards to the optimum demihull spacing and the optimal pressure patch width. The situation is complicated even further when we consider that the total resistance of an SES also depends on the parameter τ.

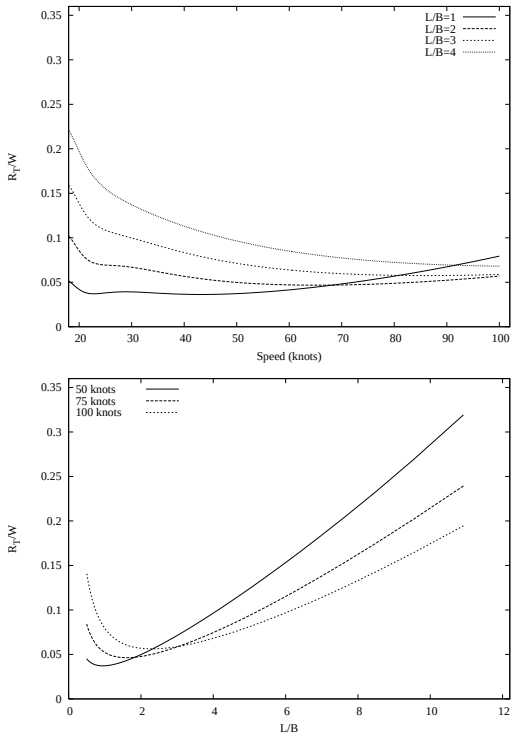

Figure 21: Specific resistance of 76.41m ACV for four length-to-beam ratios (top) and effect of length-to-beam ratio on specific resistance coefficient at three design speeds (bottom).

5 OPTIMISATION

5.1 Memetic Algorithms

Many engineering design tasks can be cast into the form of optimisation problems. One formulation, of sufficient generality for many applications, is to minimise a real-valued function $f(x_1, x_2, ..., x_n)$, with each real parameter x_i subject to (domain) constraints $a_i \leq x_i \leq b_i$ for some real constants a_i and b_i. In the context of the present thesis, f is the total resistance. Constraints can be imposed on, among other quantities, ship length and width, hull shape and, for multihulls, the location of outriggers.

Many techniques exist for solving optimisation problems such as the one described above, but they vary greatly in efficiency and the quality of the final solution for a given number of function evaluations. No single technique is best for all design problems. Gradient-based methods work well with smooth, unimodal functions, but may yield local optima for multimodal functions. Heuristic algorithms can increase search efficiency, but at the expense of guaranteed optimality - they do not always find the global optimum.

Genetic Algorithms (GA) are adaptive search methods that use heuristics inspired by natural population dynamics and the evolution of life. They differ from other search and optimisation schemes in four main respects, Dhingra and Lee [12]. Search proceeds from a population of points, not from a single point; they use a coding of the parameters, not the parameters themselves; objective function values guide the search process - they do not use gradients or other problem-specific information; state transition rules are probabilistic, not deterministic.

While they are quite effective techniques for global optimisation, GA can sometimes take an intolerably long time to converge. In short, both GA and local search techniques can spend disproportionate amounts of effort examining infeasible regions of the (often enormous) search space. GA sometimes search too broadly, local search methods too narrowly.

Many different methods have been devised combining GA with other search techniques in an attempt to improve their overall performance. The evolutionary biologist Richard Dawkins coined the word "meme" (rhyming with cream) as a term for non-material entities that are capable of transmission or imitation, such as ideas, tunes, and catch–phrases [7]. Memetic algorithms are GA that incorporate local search techniques.

5.2 Computer Techniques

"GODZILLA" is an optional addition to the present author's computer program Michlet which implements a non-traditional GA similar to Eshelman's [22] "CHC" algorithm. The system has been enhanced with additional heuristics such as cataclysmic restarts, and incest prevention, described in Eshelman and Schaffer [23].

GODZILLA's general operation can be described quite succintly: create and evaluate new (candidate) designs until some termination criterion is met. In the present thesis, a run is terminated when a certain fixed number of designs have been evaluated. There are no theoretical results that can be used to determine the optimum number of evaluations that should be performed.

GODZILLA begins the optimisation process by creating an initial population of real-valued design vectors and calculating the total resistance for each design. In the present thesis, initial designs are randomly generated.

Genetic operators and other heuristics are used to create candidate designs. Genetic operators create new (offspring) vectors from two parent vectors in the population, using heuristics inspired by the recombination of DNA. The primary genetic operator in GODZILLA is based on an operator gleaned from fuzzy set theory as described in Voigt et al [80].

GODZILLA uses "binary tournament selection" to select parent vectors from the population. In this method, two individuals are selected without replacement from the population. The individual with the lower total resistance becomes the first parent. A second binary tournament determines the other parent.

After evaluating the total resistance of the offspring, GODZILLA replaces another individual in the population with the offspring if the offspring's total resistance is lower. This replacement strategy guarantees that the best individual in the population is never replaced by an inferior individual.

Stochastic search techniques can place great demands on computer resources. It is important to run a sufficient number of cases, each time varying only the initial population, in order to enable some confidence that an optimal solution has been found, or at the least that it has been well-approximated. Just as importantly, each run must be allowed to continue for long enough to be able to find the optimal solution, but not for too long so that resources are wasted. Unfortunately, there are no theoretical results available that allow reasonable estimates to be made for the required duration, nor of the number of runs required to guarantee that an optimal solution has been found.

6 OPTIMISATION OF A 1200T VESSEL

The task in this example is to find choices of geometric parameters, subject to a variety of practical constraints, that minimise the total calm-water resistance of a 1200 tonne laterally symmetric vessel at two design speeds, 50 knots and 75 knots.

6.1 Constraints

The constraints imposed on all vessels in this example are based on the principal dimensions of the 1200 tonne INCAT86 catamaran built by International Catamarans Pty Ltd. This vessel is about 76.41m long, 26.0m wide, and with a maximum draft of about 3.5m.

All vessels in the present example have a (fixed) overall length, LOA, of 76.41m. For trimarans we impose the further restriction that either the central hull or the outriggers (or both) must have length 76.41m. This constraint is intended to exclude multihull arrangements with excessive longitudinal stagger. The maximum overall width of all vessels is 26.0m, a constraint chosen to prevent excessively wide vessels which would be difficult to manoeuvre and to load and unload in port. The maximum draft allowed during the optimisation is 3.5m. The minimum allowable overall transverse metacentric height ($\overline{GM}_{TOA}$) is 1.0m.

6.1.1 Monohull constraints

Constraints imposed on the 1200 tonne monohulls are summarised in Table 10. The first five parameters (L to f_2) are, with the displacement volume, ∇, "primary" input quantities: they are all that are needed to specify the complete underwater shape of the hull. Constraints on these quantities are deemed to be "primary constraints"; all other constraints are referred to as "secondary" constraints.

During the optimisation process, the length L is fixed at 76.41m. The draft T is allowed to vary between 0.01m, an arbitrary lower limit, and 3.5m, a reasonable upper limit based on the depth of many Australian harbours. Waterlines are always parabolic ($f_0 \equiv 1$), but the other two shape factors are allowed to vary from rectangular to parabolic ($0 \leq f_1 \leq 1$ and $0 \leq f_2 \leq 1$).

The hull beam B is calculated from primary parameters and is thus deemed to be a "secondary" parameter. It is allowed to vary from 0.1m,

Parameter	Min.	Max.
L	76.41	76.41
T	0.10	3.50
f_0	1.00	1.00
f_1	0.00	1.00
f_2	0.00	1.00
B	0.10	26.00
L/B	5.00	50.00
B/T	0.10	10.00
L/T	5.00	50.00

Table 10: Constraints for a 1200 tonne monohull.

an arbitrary lower limit, up to 26.0m, the maximum width of any vessel permitted in this example.

The upright stability of the hull as measured by the transverse metacentric height, $\overline{GM}_T$, must be greater than 1.0m. No upper limit for $\overline{GM}_T$ is specified, however in the computer program a large value, (eg 999999.9) is imposed.

The last three secondary constraints impose limits on certain geometric ratios. The hull length-to-beam ratio, L/B, can vary between 5.0, which is an arbitrary lower limit based on, among other considerations, the practical limitations of thin-ship theory, and 50.0, which is a reasonable upper limit to prevent excessive "hull whipping", and other structural problems. The hull beam-to-draft ratio, B/T, is allowed to vary between 0.1 and 10.0, which are arbitrarily chosen to prevent unusually thin, or unusually flat, hullforms.

The limits on L/T are based on two main considerations. The first reason is for structural reasons similar to those imposed on L/B. The second reason stems from the present author's previous experience with ship optimisation, and deserves explanation as it sheds light on some of the difficulties we can anticipate during the optimisation procedure.

In general, it is possible for two monohull vessels to have the same total resistance but different proportions of viscous and wave resistance (ignoring other components for the moment). For example, a short stubby vessel has relatively low surface area and therefore relatively low skin-friction; its wide

beam though, means that it has relatively high wave resistance. It is not too difficult to conceive of another longer, thinner vessel with the same displacement volume, that has a larger surface area (and therefore more skin-friction) but lower wave resistance due to a narrower beam.

In an investigation of unconstrained multihulls, Tuck and Lazauskas [69] found that at high speeds, optimal hulls sometimes tended to be very short and very deep. Interestingly, this change in preference from a long, thin hull at one speed to a short, deep hull at another, could occur over a quite small change in design speed. Tuck and Lazauskas [69] found that adding a form factor seemed to cure the problem, (if it can indeed be called a "problem"). In fact, the imposition of the additional resistance only moved the speed at which the change in preference from long to short occurred to a higher value. The form factor we [69] employed was an empirical formula devised by Scragg and Nelson [57] during their investigation of rowing shells and is based on the angle of the hull at the bow and at the stern. In the present thesis, we will not use additional form factors because they are still so poorly understood. Instead, we have chosen to impose limits on hull draft and other geometric parameters to exclude very unconventional hull forms.

With the constraint set described above, we have a three-parameter optimisation problem: we are free to choose only the draft, T, and two shape parameters, namely f_0 and f_1.

6.1.2 Catamaran constraints

The demihulls of catamarans are subject to the same constraints as the monohull given in Table 10. The demihull lateral separation is constrained to lie in the range $21.67\text{m} \leq w \leq 26.0\text{m}$. Thus for catamarans we have a four-parameter optimisation problem: in addition to the three parameters required for monohulls, we must also find the lateral separation distance, w.

6.1.3 Trimaran constraints

The demihulls of trimarans are subject to the same constraints as the monohull. The optimisation problem thus has eleven parameters: two hull lengths, two drafts, two shape factors for the central hull, two shape factors for the outriggers, one lateral separation distance, one longitudinal separation distance, and the proportion of displacement that is in the outriggers (i.e. σ). The same limits on the lateral separation distance, w, as for catamarans

apply to the outriggers.

The longitudinal demihull separation distance is constrained to lie in the range $0.0\text{m} \leq s \leq 38.21\text{m}$. This range is only half the maximum allowable hull length because of symmetry considerations, the constraint on LOA, and because we do not allow the outriggers to extend past the bow or stern of the central hull. Symmetry allows us to halve the range because the wave resistance of a multihull vessel with fore-aft symmetric demihulls is, in Michell theory, the same whether the vessel is travelling forwards or backwards.

6.1.4 SES constraints

A comprehensive optimisation of SES should include interference effects between the pressure distribution and the demihulls, however this level of optimisation is probably more appropriate during the refinement of a design rather than at the preliminary stage.

In the present example, only the demihulls of SES are optimised. The length and width of the pressure distribution are fixed at 76.41m and 21.67m, respectively. Shape parameters for the demihulls of SES are subject to the same constraints as catamarans, except that the keel-line is rectangular (i.e. $f_2 \equiv 0$) in order to prevent leakage of air from under the sidewalls. The demihull lateral separation distance is fixed at 21.67m, which is the same width as the pressure distribution. Thus for SES we have a three-parameter optimisation problem: we must find the optimal draft, T, and two shape parameters, f_0 and f_1.

Once the optimal demihull parameters have been found, the total resistance of the SES is calculated for different values of τ, the fraction of displacement supported by the air cushion. The total resistance includes interference effects between the demihulls and the pressure distribution; however the optimisation was performed only on the demihulls.

6.1.5 ACV constraints

The overall width of an ACV is fixed at 26.0m; thus there is no optimisation to be performed for this class of vessel. The performance of ACV for other length-to-width ratios is shown in Figure 21, discussed previously.

6.2 Optimisation Procedure

The generalised trimarans in the present example were optimised for different values of the displacment ratio σ: 35 values of σ were used at 50 knots; 36 designs were optimised at 75 knots. In the first instance, we optimised for twenty-one values of σ, e.g. $\sigma = 0.0, \sigma = 0.05, \sigma = 0.1, ..., \sigma = 1.0$. Results for these optimisations were plotted and inspected, and then additional values of σ were chosen.

Each of the 71 designs was run at least seven times. An average of about 20,000 objective function evaluations were performed during each run. Thus about 100 million vessels (not all unique) were evaluated to produce the figures in the results to follow. Optimisations runs were performed on a 2.6GHz laptop computer with 256Mb of memory.

6.3 Constrained Generalised Trimarans

6.3.1 Optimal resistance components

Figure 22 shows the specific resistance as a function of σ for the optimal generalised trimarans. In this figure, and others to follow, a curve has been drawn through all values except the monohull. The apparent unusual behaviour of the monohull relative to the other vessels is due to the constraint on $\overline{GM}_T$. It is relatively easy for multihulled vessels to achieve the minimum $\overline{GM}_T$: monohulls can only achieve the same minimum by increasing beam with an attendant large increase in wave resistance.

It is clear from the two plots in Figure 22 that specific resistance varies quite differently with σ for the two design speeds.

For a design speed of 50 knots, the monohull has by far the worst resistance. The total resistance of trimarans with small outriggers, $0 < \sigma < 0.12$, is about 7% less than the monohull. As σ increases from 0.12, the total resistance decreases smoothly to a (local) minimum at about $\sigma \approx 0.65$, at which point all three hulls have roughly the same displacement. As σ increases from 0.65 up to $\sigma \approx 0.95$, the total resistance increases. For this range of σ the vessel is essentially a catamaran with a small central hull. Since the small central hull can do little to cancel waves created by the large outriggers it is, in a sense, parasitic. As σ increases from a value of 0.95, i.e. as the central hull becomes even smaller, the resistance decreases to a minimum when $\sigma = 1.0$, i.e. when we have a "pure" catamaran, which is the best choice for the 50 knot design speed.

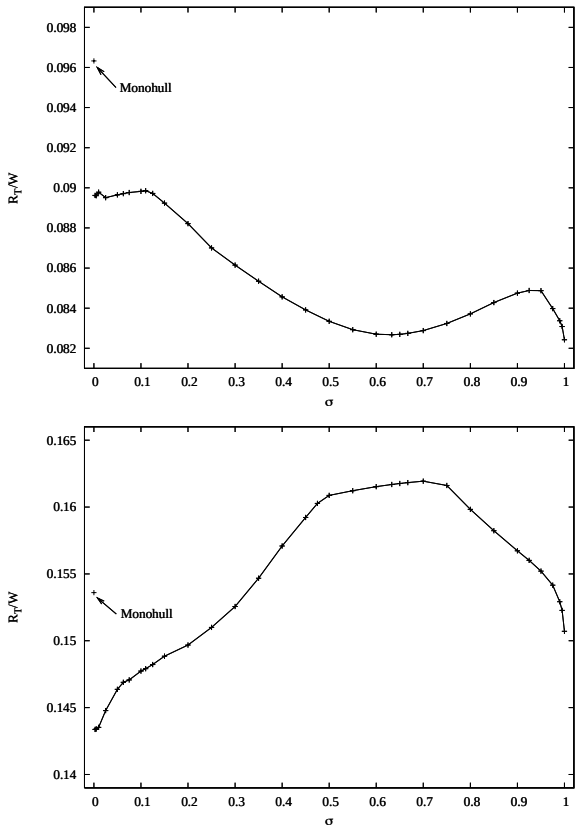

Figure 22: Specific resistance of generalised trimarans optimised for minimum hydrodynamic resistance at 50 knots (top) and 75 knots (bottom).

For a design speed of 75 knots, the optimal monohull has about 7% greater resistance than the trimaran with the smallest outriggers that were allowed during the optimisation (i.e. $\sigma \approx 0.001$). The total resistance increases smoothly as σ increases, reaching a maximum at $\sigma \approx 0.7$ when all three hulls have about the same displacement. It is interesting to contrast this with the 50 knot designs for the same range of σ. As σ increases from 0.7, total resistance decreases smoothly to a (local) minimum at $\sigma = 1.0$.

Trimarans with small outriggers are clearly the best choice for the 75 knot design speed. We can do better than the monohull by using any trimaran with $\sigma < 0.32$: the catamaran is inferior to (true) trimarans with $\sigma < 0.25$.

The resistance components of the optimal vessels at the two design speeds are shown in Figure 23.

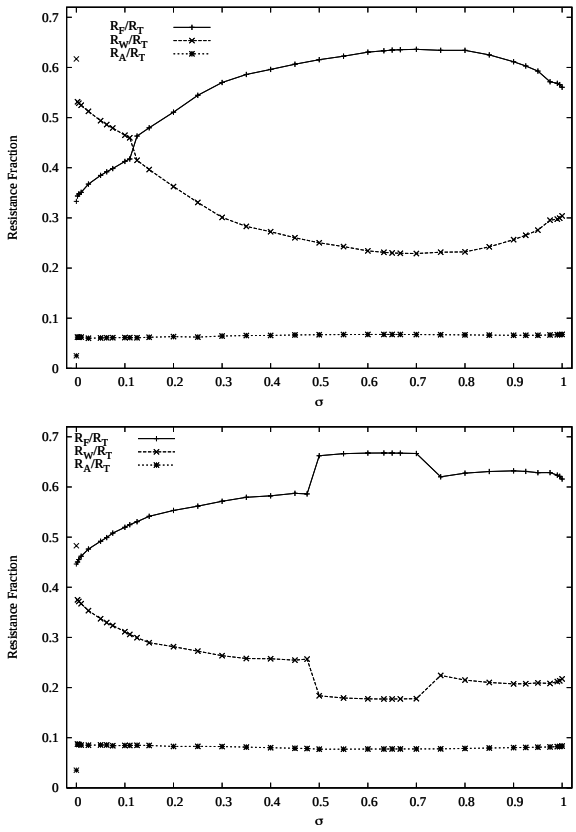

Figure 23: Resistance components of generalised trimarans optimised for minimum hydrodynamic resistance at 50 knots (top) and 75 knots (bottom).

Air resistance comprises the smallest fraction of the total for both design speeds. At a design speed of 50 knots, air resistance comprises only about 2% of the total for monohulls and about 7% for multihulled vessels. At 75 knots, air resistance comprises about 3% for monohulls and about 8.5% for multihulls. The smaller above-water frontal area of the monohulls is responsible for the lower fraction.

At a design speed of 50 knots, wave resistance comprises the largest fraction of the total for monohulls and for trimarans with small outriggers ($0 \leq \sigma \leq 0.11$). The resistance of vessels with larger outriggers ($\sigma > 0.11$) is dominated by frictional resistance which varies between about 45% and 62% of the total.

At 75 knots, frictional resistance comprises the largest fraction for all

vessels except the monohull. For trimarans with large outriggers ($0.5 \leq \sigma \leq 0.75$) the frictional component makes up about 65% of the total. As we will see in the next section, the optimal vessels for this range of σ have three hulls of approximately the same length. Thus, although the demihulls are quite thin and produce relatively small waves, they have a relatively large surface area and hence large skin-friction.

6.3.2 Optimal geometric parameters and off-design performance

Optimal geometric parameters and off-design performance for the vessels found during the optimisation are presented in Figures 24 to 31. In the interests of brevity, results are shown only for the most important geometric parameters. The discussion of each figure is given in the caption attached to the figure.

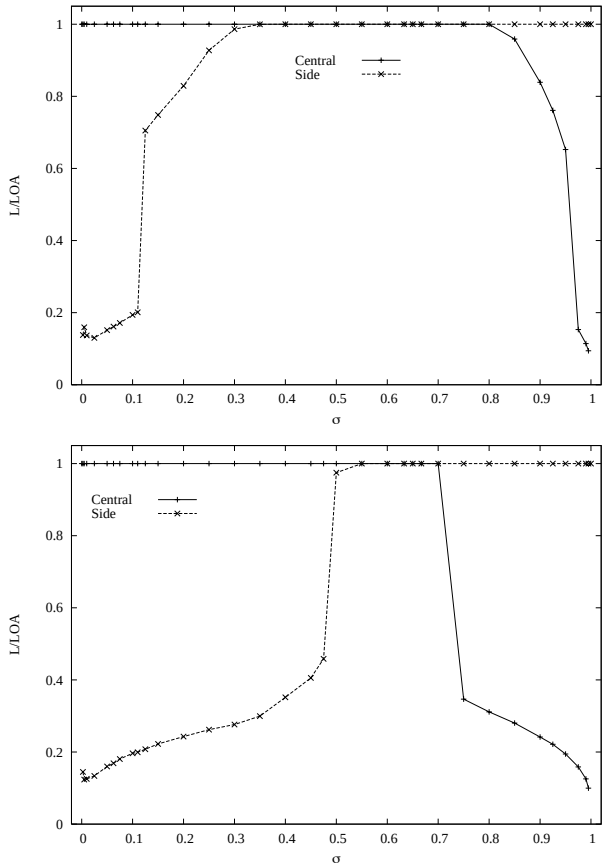

Figure 24: Hull length ratios of generalised trimarans optimised for minimum hydrodynamic resistance at 50 knots (top) and 75 knots (bottom). For a design speed of 50 knots the central hull has the maximum allowable length for $\sigma < 0.8$. For larger σ the central hull length decreases smoothly until, at $\sigma = 1.0$ (i.e. when we have a catamaran) it vanishes For $\sigma < 0.11$ the sidehull lengths are less than 20% of the overall length. At 75 knots, the optimal sidehull lengths remain shorter for a wider range of σ than for the 50 knot designs.

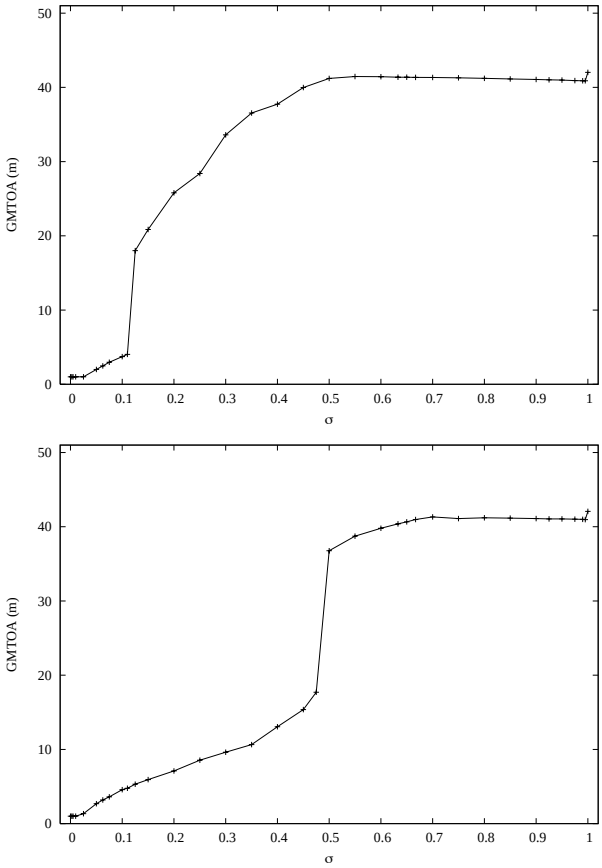

Figure 25: Transverse metacentric height of generalised trimarans optimised for minimum hydrodynamic resistance at 50 knots (top) and 75 knots (bottom). For both design speeds, $\overline{GM}_T \approx 1.0$m for the monohull and for trimarans with very small outriggers ($0 \leq \sigma < 0.02$). For the 50 knot designs, $\overline{GM}_T$ increases slowly until σ reaches about 0.11, at which value it then increases very rapidly when the sidehull length increases). For $0.5 < \sigma < 1$, $\overline{GM}_T$ remains almost constant at about 41.0m. The value for the catamaran is slightly higher. For the 75 knot designs $\overline{GM}_T$ increases smoothly until $\sigma \approx 0.47$ at which value it jumps suddenly to a value of about 41.0m when the sidehull length increases sharply. If large metacentric heights (say $\overline{GM}_T > 5.0$m) are undesirable because of concerns with passenger comfort, the range of acceptable vessels is quite small. For both design speeds our choice is limited to the monohull and to trimarans with small outriggers, i.e. to the range $0 \leq \sigma \leq 0.11$.

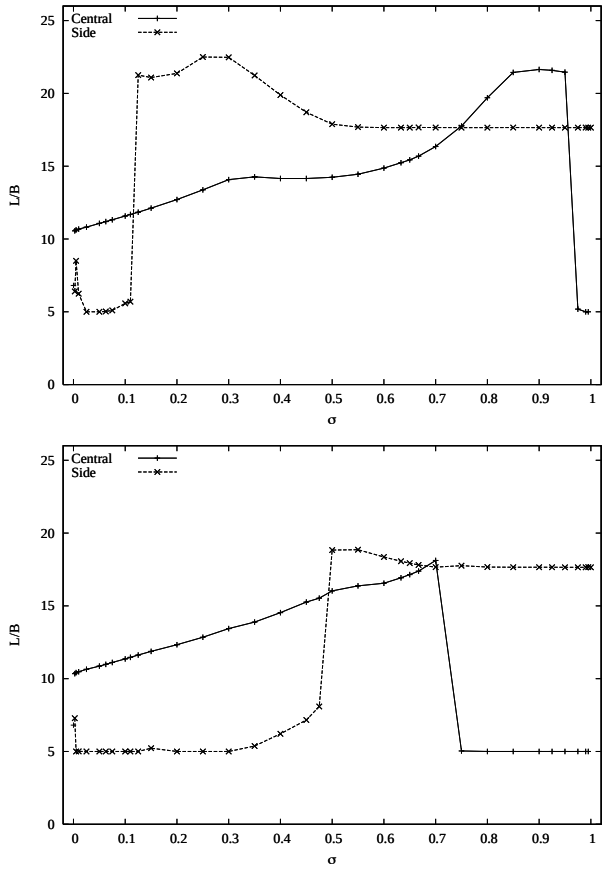

Figure 26: Hull length-to-beam ratios of generalised trimarans optimised for minimum hydrodynamic resistance at 50 knots (top) and 75 knots (bottom). For both design speeds the monohulls have a length-to-beam ratio of about 7.0. The length-to-beam ratio of small outriggers (i.e. when $\sigma \approx 0.05$) is the minimum allowed during the optimisation.

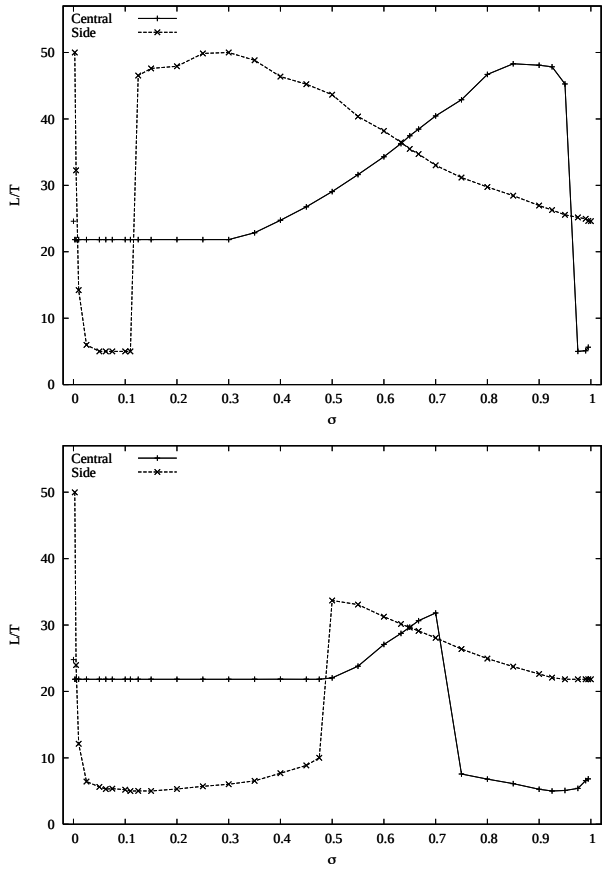

Figure 27: Hull length-to-draft ratios of generalised trimarans optimised for minimum hydrodynamic resistance at 50 knots (top) and 75 knots (bottom). For both design speeds the monohulls have a length-to-draft ratio of about 24.0. The length-to-draft ratio of small outriggers (i.e. when $\sigma \approx 0.05$) is the minimum allowed during the optimisation.

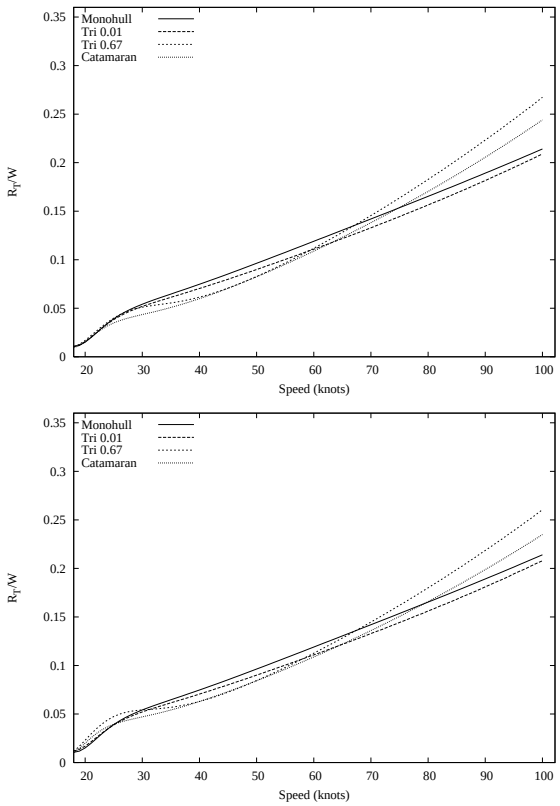

Figure 28: Off-design specific resistance of four generalised trimarans optimised for minimum hydrodynamic resistance at 50 knots (top) and 75 knots (bottom). Of the 50 knot designs shown at the top of the figure, the catamaran has the lowest drag for speeds up to about 62 knots; Tri 0.67 is not much worse between 45 knots and 55 knots. The monohull and Tri 0.01 are not competitive at low speeds. Tri 0.01 is the best of the 75 knot designs for speeds greater than 63 knots, but it is not as good as the catamaran at lower speeds. Tri 0.67 has quite good characteristics for speeds between 40 knots and 50 knots, however it is by far the worst performer for speeds between 20 knots and 30 knots.

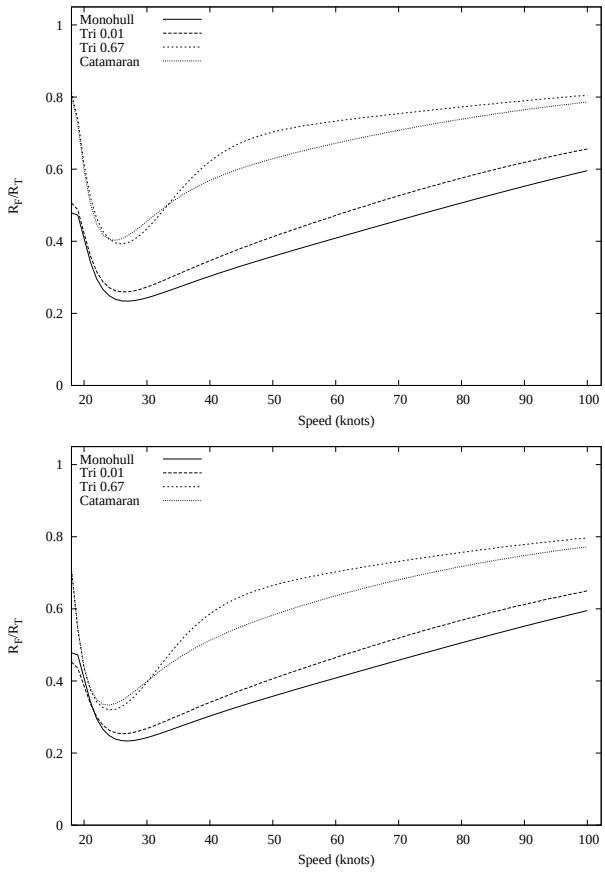

Figure 29: Off-design friction resistance fraction of four generalised trimarans optimised for minimum hydrodynamic resistance at 50 knots (top) and 75 knots (bottom). As expected, frictional resistance is the most significant component of the total drag for the catamaran and Tri 0.67, the two vessels with the largest wetted surface areas.

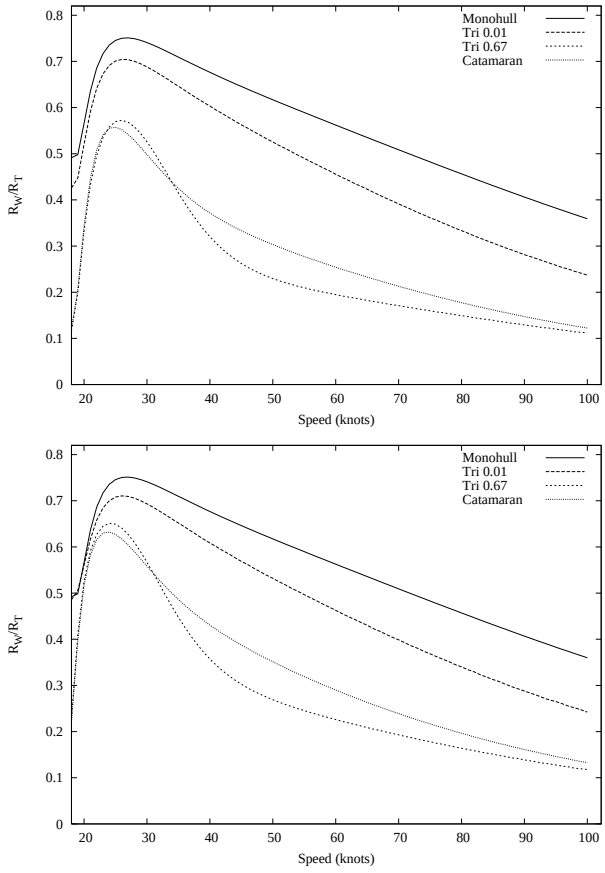

Figure 30: Off-design wave resistance fraction of four generalised trimarans optimised for minimum hydrodynamic resistance at 50 knots (top) and 75 knots (bottom). All curves have a clear maximum at about 25 knots, where the Froude number based on overall length is about 0.47. For both the 50 knot and the 75 knot designs, wave resistance is the least significant component of the total drag for both the catamaran and Tri 0.67.

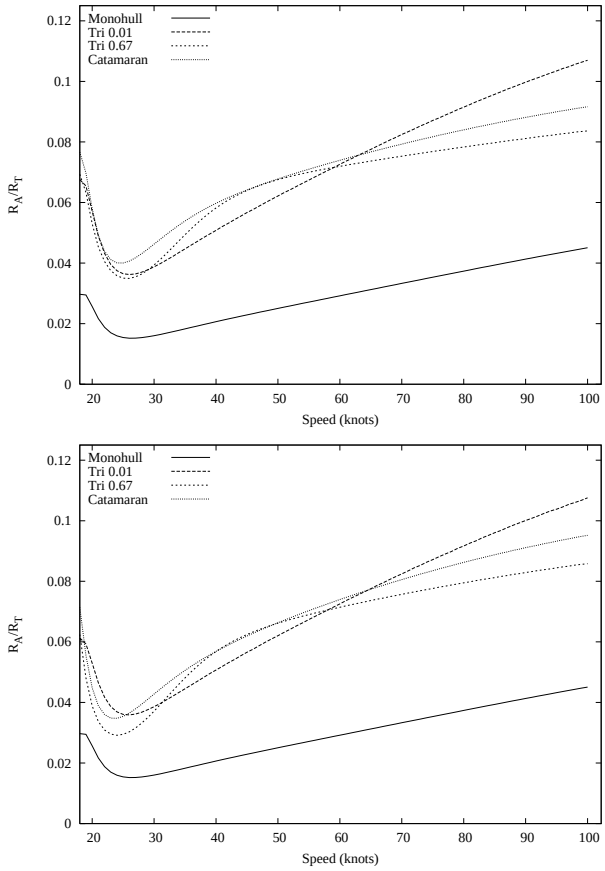

Figure 31: Off-design air resistance fraction of four generalised trimarans optimised for minimum hydrodynamic resistance at 50 knots (top) and 75 knots (bottom). It can be seen that air resistance comprises a relatively small component of the total drag for both the 50 knot and the 75 knot designs. This in part justifies the optimisation procedure whereby we optimised vessels for the hydrodynamic drag only, and then added the air resistance. The fraction of air resistance increases smoothly for all vessels from a minimum at about 25 knots, where wave resistance is generally the largest component. For both the 50 knot and the 75 knot designs, air resistance is much less significant for the monohull than for the multihulls because of the monohull's smaller frontal area.

6.4 Constrained SES

As mentioned before, optimisation of SES was performed only for the catamaran portion of the vessel at full displacement, i.e. when the demihulls support the 1200 tonnes and there is no cushion pressure.

6.4.1 Optimal resistance components and off-design performance

Optimal resistance components and off-design performance for the SES designs are given in Figures 32 to 37. The discussion of each figure is given in the caption attached to the figure.

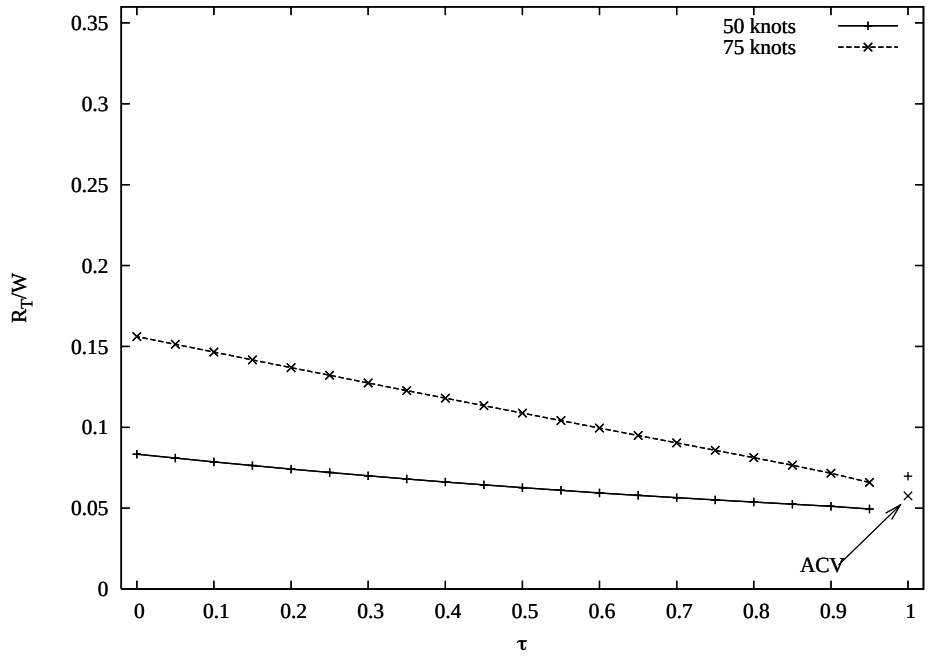

Figure 32: Specific resistance of generalised SES at two design speeds. τ is the fraction of displacement supported by the air cushion. It is clear that for both design speeds total resistance decreases smoothly from a maximum at $\tau = 0$ to a minimum at $\tau = 0.95$. The resistance of the the ACV ($\tau = 1.0$) at 50 knots is larger than the $\tau = 0.95$ SES, however at 75 knots the ACV is superior.

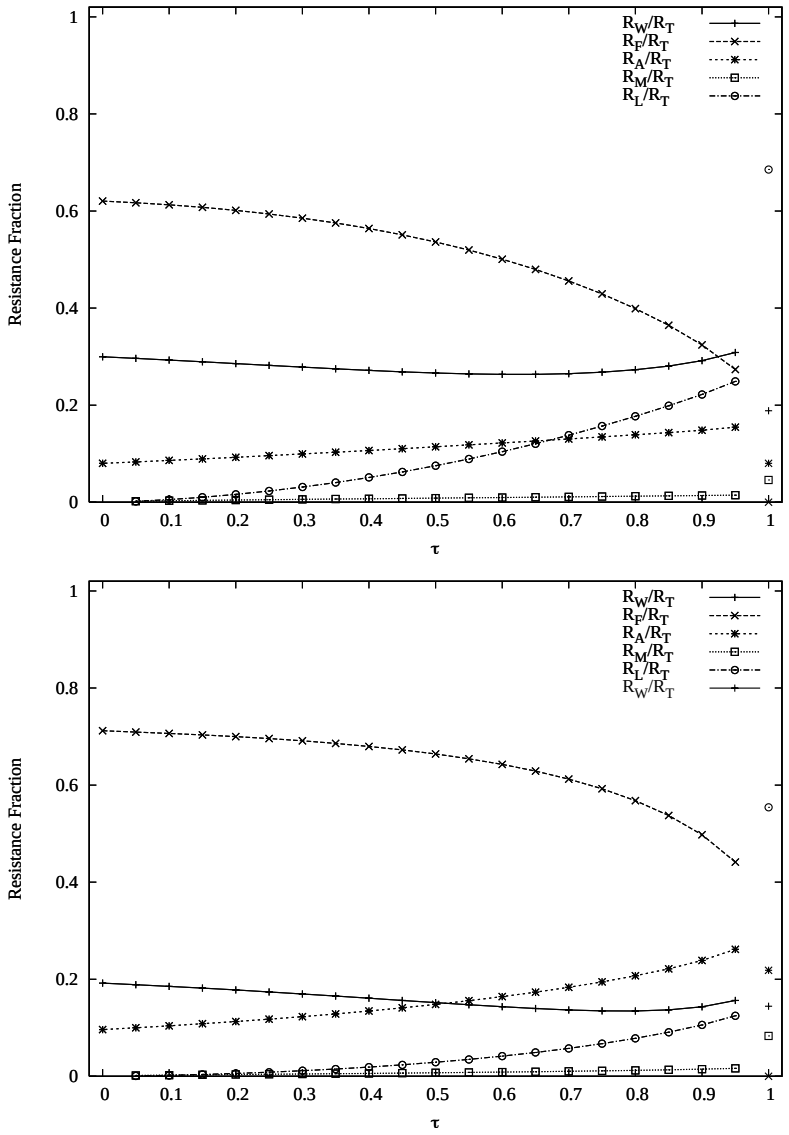

Figure 33: Resistance components of generalised SES at 50 knots (top), and 75 knots (bottom). Frictional resistance is the dominant component of the total drag for all SES, except for the 50 knot SES with $\tau > 0.92$. Equivalent lift is the dominant component of the total drag of ACV, comprising about 70% at 50 knots, and 55% at 75 knots. Air resistance is the second largest component of the total for all 75 knot designs with $\tau > 0.52$. Momentum resistance is, by far, the least significant component of the total drag for all vessels. It is somewhat smaller for SES than for ACV which have a much larger perimeter from which air can escape. (See equations 24 and 25).

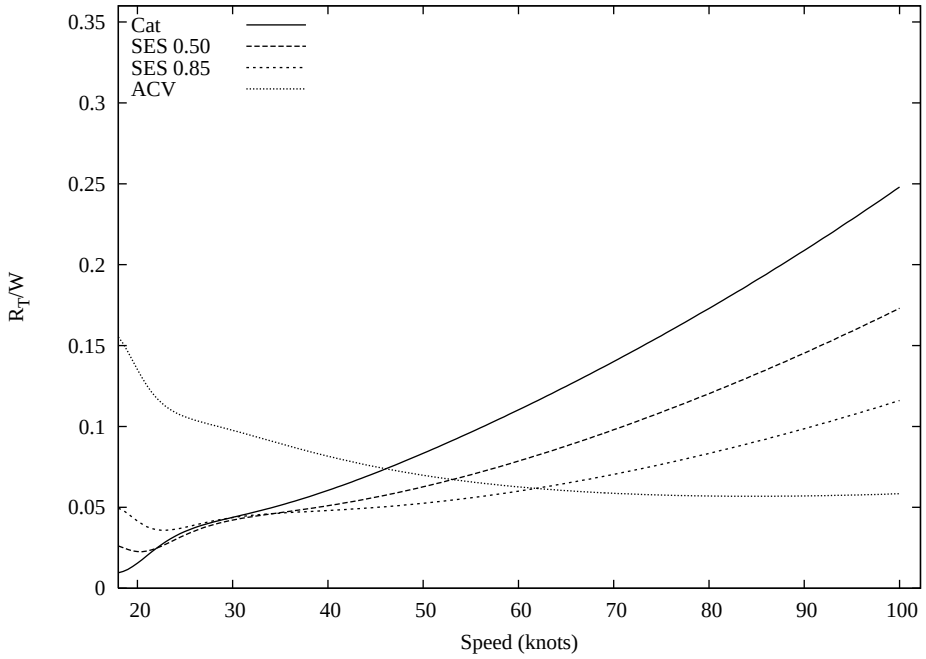

Figure 34: Off-design specific resistance for generalised SES. The catamaran (here an SES with $\tau = 0.0$) is not competitive with the other vessels for speeds greater than about 25 knots. The ACV has the largest total resistance of all four vessels for speeds below about 45 knots, however it is the best vessel for speeds greater than about 62 knots. The figure suggests a promising hybrid vessel. Below about 20 knots, the vessel should behave like a catamaran. As speed increases, we should lift part of the vessel out of the water by increasing the cushion pressure, until at 62 knots the hulls are no longer submerged and the vessel is, for all intents, a "pure" ACV. It is an open question whether an efficient propulsion system can be devised for all three modes of operation.

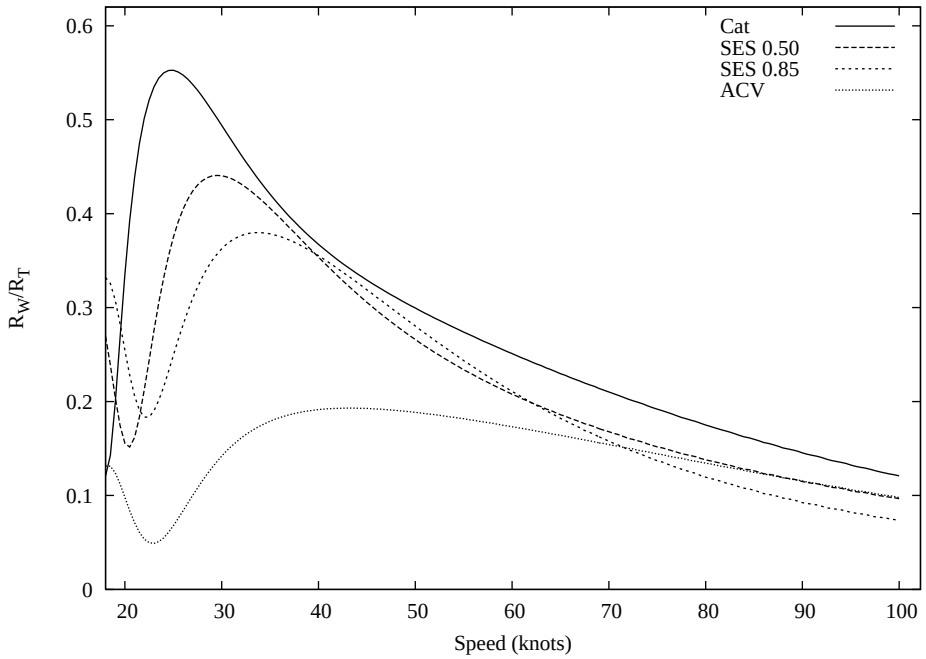

Figure 35: Off-design wave resistance fraction (bottom) for generalised SES. The wave resistance fraction reaches a maximum at different speeds depending on the amount of displacment supported by the air cushion. For an SES in catamaran mode (i.e. $\tau = 0$), wave resistance comprises about 55% of the total at about 25 knots. Maxima are attained at about 30 knots for the SES 0.50; and at 33 knots for the SES 0.85. The maximum fraction for the ACV occurs at about 42 knots.

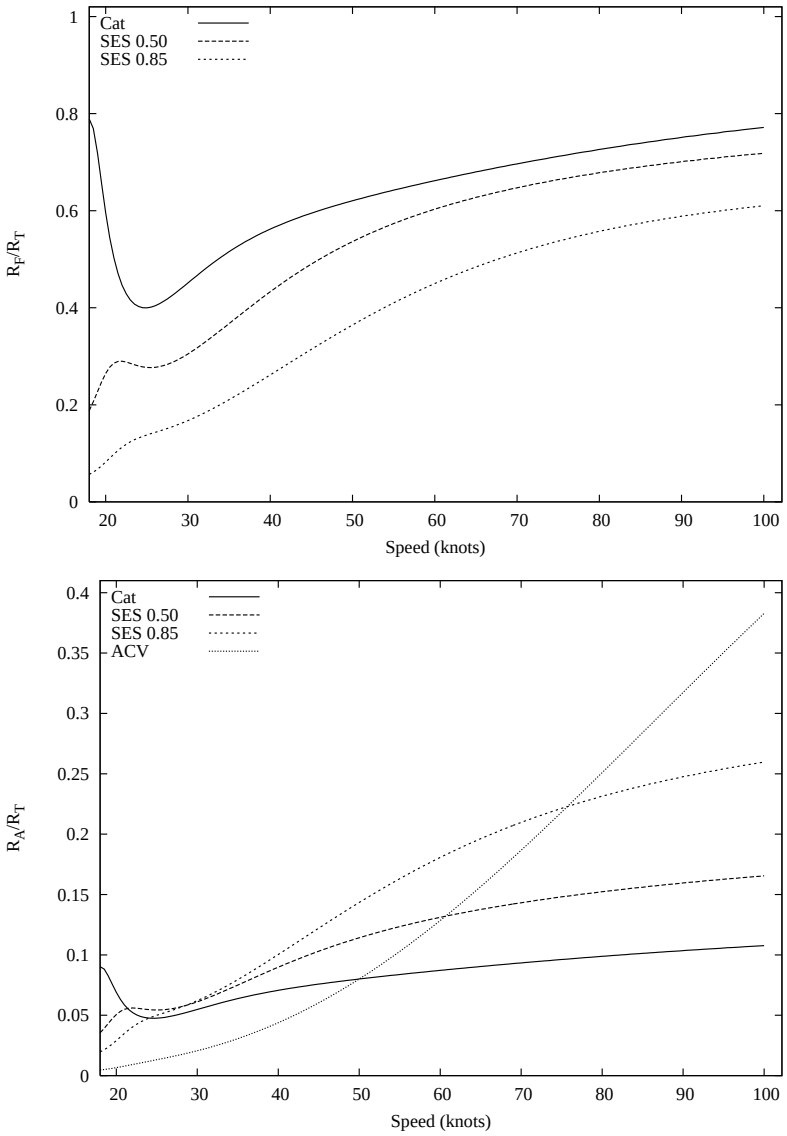

Figure 36: Off-design friction resistance fraction (top) and air resistance fraction (bottom) for generalised SES. The top figure shows that skin friction comprises more than half of the total drag of a catamaran for speeds greater than about 33 knots. The bottom figure shows the increasing significance of air resistance for ACV as speed increases. At 50 knots it comprises about 7% of the total, at 75 knots about 22%, and at 100 knots it makes up about 38%.

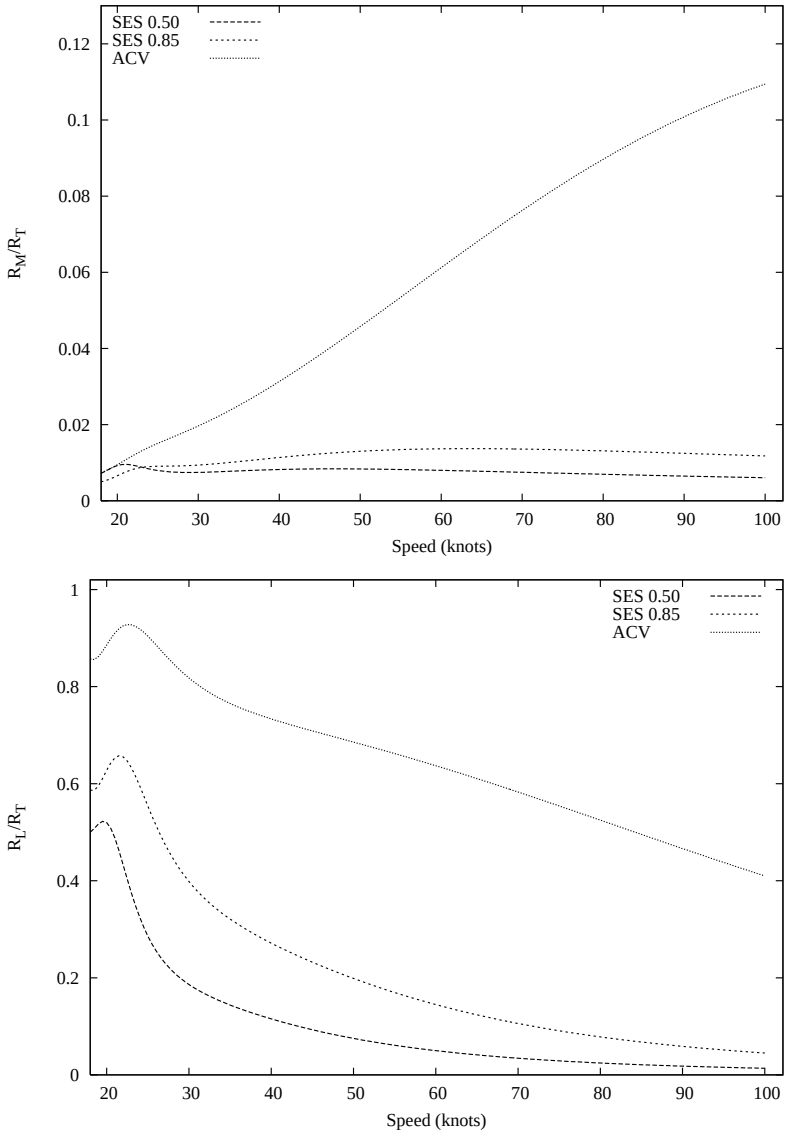

Figure 37: Off-design momentum air resistance fraction (top) and equivalent lift resistance fraction (bottom) for generalised SES. The top figure shows that momentum resistance makes up roughly 1% of the total drag of the two SES for all speeds. This component is more significant for the ACV where it comprises about 4% at 50 knots, 8% at 75 knots, and 11% at 100 knots.

6.5 Comparison of Optimal Vessels

We now select for further investigation six vessels that are representative of the classes we optimised previously. The $\sigma = 0.01$ vessel will be used to represent the class of trimarans with small sidehulls. In effect, these vessels are just very slender monohulls that employ small outriggers to achieve the minimum transverse metacentric height $\overline{GM}_{TOA}$ required during the optimisation. Any vessel with $0.0 < \sigma < 0.1$ could have been used.

Vessel	R_T/W at 50 kts	Rank	R_T/W at 75 kts	Rank
Monohull	0.0963	6	0.1536	5
Trimaran ($\sigma = 0.01$)	0.0900	5	0.1443	3
Trimaran ($\sigma = 0.67$)	0.0828	4	0.1620	6
Catamaran	0.0825	3	0.1506	4
SES ($\tau = 0.85$)	0.0525	1	0.0765	2
ACV	0.0698	2	0.0576	1

Table 11: Specific resistance of a selection of vessels optimised for minimum hydrodynamic resistance and their ranking (1 =best, 6 =worst).

Table 11 shows the specific resistance of six vessel types. Also shown in the table are the rankings of the vessels, with 1 signifying the vessel with the lowest total resistance, and 6 indicating the highest.

On the basis of lowest total resistance, the obvious choices are an SES for a design speed of 50 knots, and an ACV for a design speed of 75 knots. Of the "pure" displacement vessels, the catamaran is best at 50 knots and the Tri 0.01 at 75 knots.

6.5.1 Powering requirements

We assume that waterjets are used for all vessels except the ACV where they are impractical. We assume that the ACV employs fully-submerged propellers (perhaps housed in pods under the skirts).

We remain silent in this work on how the propulsors are deployed, and assume that the overall efficiency of the propulsors is as given in Figure 38.

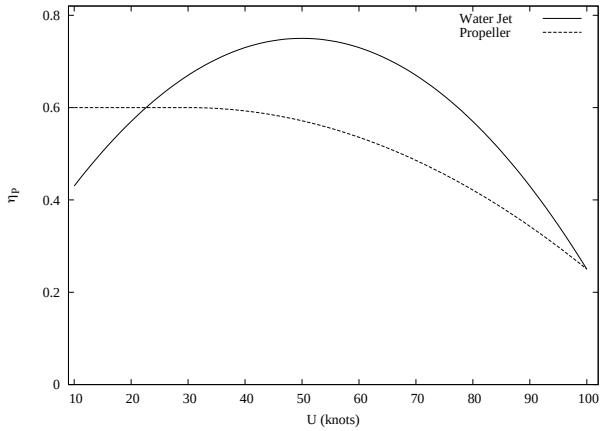

Figure 38: Assumed overall propulsive coefficients for water jets and fully-submerged propellers.

The two curves in Figure 38 are approximations to the curves given in Figure 23 of McKesson's [43] survey of the state of development of propulsors for high–speed vessels. We assume that waterjet efficiency is given by

$$\eta_p = 0.75 - 0.0002(U - 50)^2 \tag{29}$$

where the ship speed U is in knots. Waterjets have well-known problems operating at very high speeds, and it is possible that their efficiency is lower than shown in Figure 38 for speeds greater than about 60 knots.

The efficiency of a fully-submerged propeller is given by

$$\eta_p = 0.6 \quad (U \leq 30 \text{ knots}) \tag{30}$$

$$= 0.6 - 0.00007142(U - 30)^2 \quad (U > 30 \text{ knots}). \tag{31}$$

It is possible that better efficiencies are achievable for the submerged propellers, but if they are housed in pods there would also be an attendant increase in hydrodynamic resistance due to the pod housing. The propulsor efficiencies assumed here are similar to those used by Sirvio and Ahlgren [59] in their examination of large slender monohulls.

Large high-speed vessels require large powerplants and it is not a straightforward task to fit them inside slender hulls without significantly compromising the hydrodynamics of the vessel. Large powerplants are heavy, which means that for the same displacement volume, a vessel must carry less fuel

or cargo. In what follows, we assume that powering requirements depend on the total resistance of the vessel, and on the efficiency of the powerplant and the propulsors.

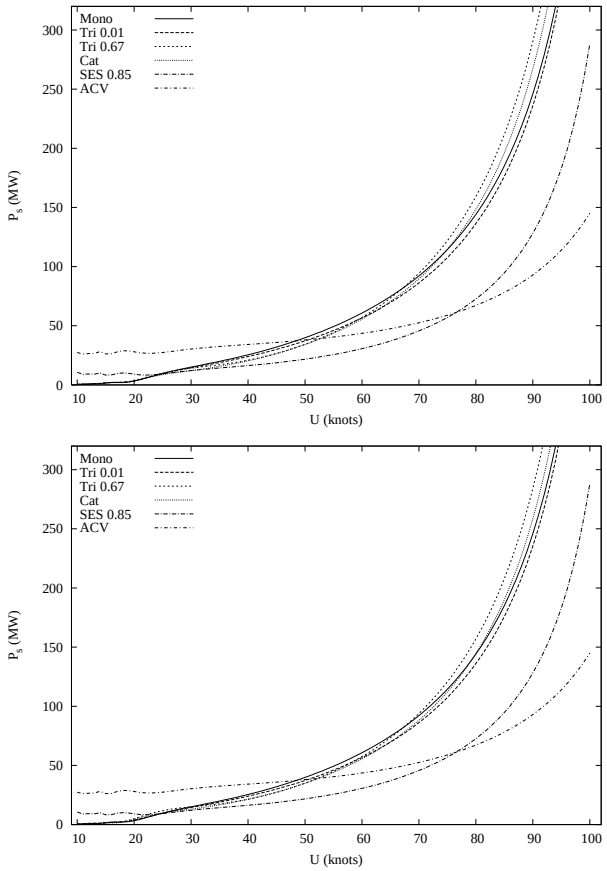

Figure 39: Shaft power as a function of ship speed: 50 knot designs (top) and 75 knot designs (bottom).

Figure 39 shows the required shaft power (in mega Watts) as a function of speed (in knots) for the six candidate vessels. (In metric units, $P_s = R_T U/\eta_p$, with R_T in Newtons, U in ms^{-1}, and P_s in Watts.)

Broadbent and Kennell [3] present a summary of the fuel consumption of several extant gas turbines, as well as predictions for the future performance of turbines. Their predictions are very similar to those of the HSST Workshop. "Far-term" performance is assumed to be achievable by the year

2008. We assume that the far-term specific fuel consumption of gas turbines is given by

$$sfc = 155 + \frac{884}{P_{smax}} \tag{32}$$

where sfc is in units of $g/kW \cdot h$ and P_{smax} is the maximum shaft power (mega Watts) required to attain the design speed. In general, fuel consumption depends on the maximum power output of the turbine and on the power at which the turbine is actually operating. Here we assume that only one turbine is required, and that equation (32) adequately models the fuel consumption in off-peak situations.

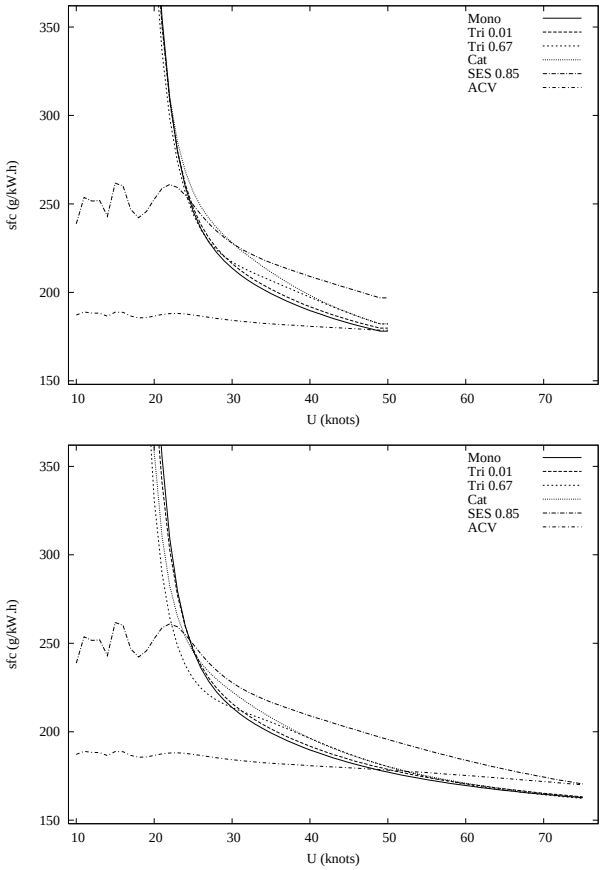

Figure 40: Specific fuel consumption of six candidate vessels as a function of ship speed: 50 knot designs (top) and 75 knot designs (bottom).

Figure 40 shows the specific fuel consumption of the six candidate vessels.

It is assumed that each vessel is equipped with gas turbines that enable them to achieve the requisite design speed.

It can be seen in Figure 40 that fuel consumption increases quite sharply as we decrease speed from the design value. For vessels that must operate over a wide range of speeds, this poor off-design consumption could well be intolerable. Diesel engines, which have a "flatter" fuel consumption curve, might then be preferable. The poor off-design fuel consumption is also an indication that high-speed vessels could be uneconomical on routes where they must spend long times in harbours, travelling at low speed. It might, in some cases, be better to split the powerplant into smaller units that have better fuel consumption for low power exertions.

6.5.2 Weight estimates

During the preliminary design stage, the weights of various components of candidate vessels can be estimated by using empirical models based on existing ships. A popular method for steel ships is that of Watson and Gilfillan, [81]. Unfortunately, their method does not translate easily to high-speed vessels constructed from modern lightweight materials such as aluminium alloys or composite plastics.

Although there is, at present, a paucity of published data for lightweight alternatives to steel, there is just enough in the literature to enable reasonable estimates to be made. As more experience is gained and more data collected, more accurate estimates will be able to be made at the early design stage.

We proceed in a fairly standard naval architectural fashion by first dividing the total weight of the vessel into several major components that can be estimated separately. Let

$$W = W_{ce} + W_c + W_f + W_m + W_o + W_s \tag{33}$$

where W_{ce} is the weight of the crew and effects, W_c is the cargo weight (or payload), W_f is the weight of fuel and oil, W_m is the weight of machinery (e.g. engines, gearboxes), W_o is the "outfit" weight, and W_s is the structural weight of the vessel.

The first three components in equation (33) are usually grouped together and referred to as "deadweight", i.e.

$$W_d = W_{ce} + W_c + W_f \tag{34}$$

The last three components in equation (33) comprise the "empty" ship (or lightship) weight, i.e.

$$W_e = W_m + W_o + W_s \tag{35}$$

Several other useful divisions of the lightship weight are possible, and for some purposes, further division is mandatory: for example, some navies require separate estimates of the electric plant, command and surveillance equipment, armaments, and auxiliary systems.

The weight of the crew and their effects, W_{ce}, is usually a small fraction of the total weight. In the present example we assume that it represents 1% of the total weight, i.e, $W_{ce}/W = 0.01$, of all vessels under our consideration.

The "outfit" weight, W_o, which includes pipes, fittings, insulation, crew accommodation, etc, depends on the vessel's purpose. For example, a vessel required to carry refrigerated cargo will have a different outfit to one that is used to transport bulk liquids. In the present example we assume that outfit represents 10 % of the total weight, i.e, $W_o/W = 0.1$, which is a reasonable estimate at the early design stage.

The weight of propulsion machinery, W_m, depends on the powering requirements of the vessel, and on the type of propulsion system. In the present example, we divide the machinery into two subcomponents, writing,

$$W_m = W_g + W_p \tag{36}$$

where W_g is the weight of the gas turbines and gearboxes, and W_p is the weight of the propulsors, e.g. water jet units, lifting fans, propellers etc.

In McKesson's, [46] survey of available ship powerplants, the best currently available gas turbine seems to be the Rolls-Royce Trent. This 47.5 MW turbine weighs 26 tonnes, and requires a 48 tonne reduction gear unit. We assume that the weight of the turbines and transmission, can be modelled by

$$W_g = 1.56 P_s \tag{37}$$

where P_s is the shaft power (in mega Watts) required to reach the design speed. An implicit assumption in equation (37) is that the weight of the powerplant is infinitely scalable to all sizes of turbines.

Note also that the power required to reach the design speed is not the same as that required to keep the ship at the design speed. Some vessels must first get over a "hump" at lower speeds before they can reach their design

speeds. Inadequate power to overcome the hump means the vessel will never attain the design speed.

The weight of the propulsion system is based on the weight of waterjet units. Karayannis et al, [36] provide a trend curve for the weight of waterjets as a function of power absorbed, but we here choose a slightly simpler, linear relationship

$$W_p = 0.85P_s \tag{38}$$

where P_s is the maximum shaft power in mega Watts. The constant is based on a 12MW waterjet unit weighing 10.2 tonnes. The implicit assumption in the model is that it is adequate for all power requirements and that only one unit is required. We also assume that the model is adequate (i.e. at the early design stage) for other propulsors such as fully-submerged propellers.

The structural weight, W_s, of the vessel includes the hull below the waterline as well as the superstructure and deck housing.

To estimate the structural weight of our candidate vessels, we use the method of Karayannis et al. [36] which is a modification of the equipment numeral method of Watson and Gilfillan [81] for steel ships. The equipment numeral for monohulls (or the central hull of a trimaran) is

$$E_1 = L(B + T) + 0.85L(H_f + H_s) \tag{39}$$

where L is the hull length, T is the draft, B is the hull beam, H_f is the height of the freeboard, and H_s is the height of the superstucture. (See Figure 4.) The first term in the equation represents the area of hull below the waterline. The second term represents the area of the hull above the waterline. The constant 0.85 is intended to account for the reduced weight of the material above the waterline because those parts of the hull are not subject to hydrostatic forces and wave loads.

The equipment numeral of a catamaran (or a pair of trimaran sidehulls) is

$$E_2 = 2L(B + T) + 0.85L(H_f + H_s) + 1.6L(\mathrm{WOA} - 2B_2 - B_1) \tag{40}$$

where L is the demihull length, T is the demihull draft, B_1 is the demihull beam of the central hull (if any), B_2 is the beam of a sidehull, and WOA is the overall width of the vessel. The third term in the equation accounts for the weight of the cross-structure connecting the sidehulls (and central hull for trimarans). The form chosen here for the cross-structure term is a

slight modification to the original method of Karayannis et al, [36] which was developed for monohulls and catamarans only. Here we have deducted from the cross-structure the effect of the central hull which is not present in a "pure" catamaran.

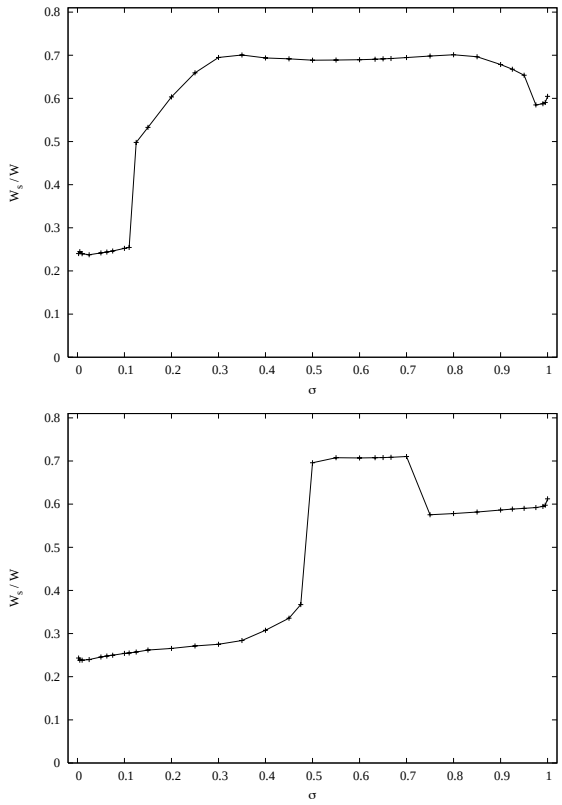

Figure 41: Structural weight fraction of generalised trimarans optimised for minimum hydrodynamic resistance at 50 knots (top) and 75 knots (bottom). Structural weight W_s includes the hull below the waterline as well as the superstructure and deck housing.

The structural weight of a monohull (or the central hull of a trimaran) is given by

$$W_1 = 0.032 E_1^{1.2}. \tag{41}$$

The constants in the equation were estimated by Karayannis et al [36] in a parametric analysis of fast aluminium monohulls with ship lengths from 50m to 125m, and length to beam ratios from 4.5 to 7.0.

The structural weight of a catamaran (or the sidehulls of a SES, or a pair of trimaran sidehulls) is given by

$$W_2 = 0.00064E_2^{1.7} \ (E_2 \leq 3025) \quad (42)$$

$$= 0.39E_2^{0.9} \ (E_2 > 3025). \quad (43)$$

Karayannis et al [36] derived the constants in the equation from a parametric analysis of fast aluminium catamarans with ship lengths of 50m, 75m and 100m.

The weight of a trimaran is $W_1 + W_2$. We assume, in the absence of published data on ACV, that their structural weight is identical to SES.

Figure 41 shows the structural weight fraction, W_s/W, for generalised trimarans optimised for minimum total hydrodynamic resistance. The weight fractions for the SES and ACV are not shown but are very similar to those of the catamarans ($\sigma = 1$).

For the 50 knot designs, it can be seen that the largest weight fractions occur for $0.15 < \sigma < 0.95$, which corresponds to those trimaran vessels where the sidehulls are of comparable length to the central hull. (See Figure 24.) For 75 knot designs, the sidehulls are of comparable length to the central hull for a narrower band of sigma, $0.5 < \sigma < 0.7$.

It is evident from the figure that the trimaran with large outriggers we have chose as a candidate vessel (i.e. Tri 0.67) has a significantly larger structural weight than the other candidates for both design speeds. Clearly, this vessel will not be able to carry as much cargo or fuel as the other vessels. The trimaran with small outriggers (Tri 0.01) has the lowest structural weight of the six candidate vessels for both design speeds. Interestingly, the monohull and the catamaran have roughly the same structural weight fractions.

6.5.3 Range

At the HSST workshop, Doctors [14] and McKesson, [44] presented empirical formulae that can be used to estimate the range of HSSV. Doctors uses the so-called Breguet formula which is a little more refined than McKesson's since it contains an additional term accounting for the fact that the total fuel weight does not have to be carried for the entire voyage. Breguet's formula is

$$s_{max} = -367098.8 \frac{\eta_p}{sfc} \frac{W}{R_T} \log_e(1 - \frac{W_f}{W}) \quad (44)$$

where s_{max} is the range in kilometers, η_p is the overall propulsive coefficient, and *sfc* is the specific fuel consumption (in $g/kW \cdot h$). R_T is the total resistance of the vessel at the speed of interest, W is the total weight of the ship, and the ratio W/R_T is referred to as the lift–to–drag ratio. W_f is the weight of fuel at the beginning of the voyage.

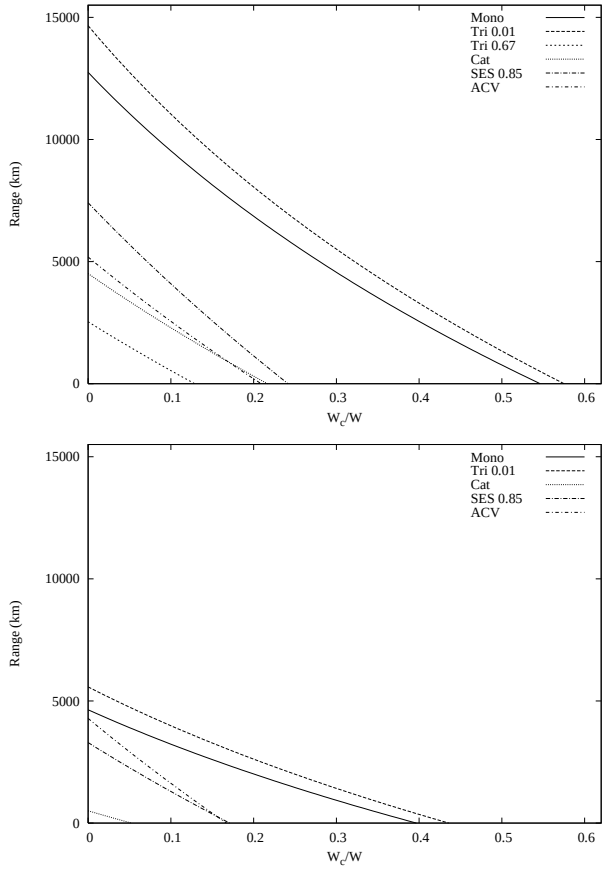

Figure 42: Range as a function of the cargo weight fraction at 50 knots (top) and 75 knots (bottom).

Figure 42 shows the range of the candidate vessels as a function of the cargo weight fraction. It is clear that Tri 0.01, the trimaran with a slender central hull and very small outriggers, can achieve the greatest range for a given cargo weight for both design speeds. The trimaran with large outriggers, Tri 0.67, is by far the worst performer. Results for this vessel are not shown in the plot at the bottom of the figure because it is unable to carry

any cargo whatsoever, i.e. the sum of the weight components of this vessel exceeds the total displacement weight. At 75 knots, the catamaran is also not competitive with the other vessels.

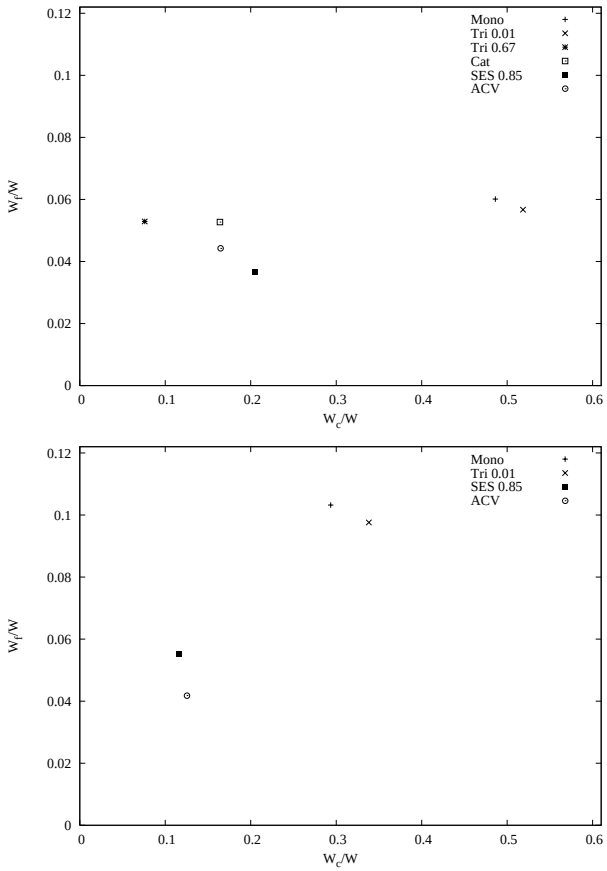

Figure 43: Fuel weight fraction required for a range of 1000 km as a function of the payload fraction for 50 knot designs (top) and 75 knot designs (bottom).

Figure 43 shows the weight of fuel that is required to achieve a maximum range of 1000 km as a function of the payload fraction. Similar plots could be made for other ranges of interest, but the general conclusions will be the same.

Of the 50 knot designs, the SES uses the least fuel to complete a voyage of 1000km, but it can carry less cargo than either the monohull or Tri 0.01. The catamaran can carry about the same payload as the ACV, but requires more fuel. The Tri 0.67 is the worst performer at this design speed.

There are only four feasible 75 knot designs: the catamaran and Tri 0.67 are both unable to carry enough fuel to complete a 1000km voyage. The ACV can carry slightly more cargo than the SES for less fuel. Tri 0.01 can carry almost three times more cargo than the ACV, but requires about 2.5 times more fuel.

7 CONCLUSIONS

This thesis examined how hydrodynamics can be used in the preliminary design and assessment of a variety of high-speed vessels including monohulls, catamarans, trimarans, SES and ACV.

Total calm-water resistance was considered to be comprised of five separate components, and the magnitude of each component was estimated by a different physics-based method. It was shown that Grigson's method for estimating skin-friction yields better estimates than the "standard" ITTC line. Wave resistance was estimated using generalisations of Michell's thin-ship theory. A simple empirical formula was derived to estimate the location of peaks and hollows in the free wave spectrum of a Wigley monohull. Another empirical formula was derived to estimate the optimum demihull separation of catamarans equipped with Wigley demihulls.

In a practical example, memetic algorithm techniques were used to find optimal geometric parameters of a 1200 tonne vessel under a variety of practical constraints. Empirical formulae were used to estimate the weight components of the vessels as well as their powering requirements. Estimates were then made of the payload capacity and the fuel consumption required for a 1000km voyage.

Many aspects of the performance of high-speed vessels were not considered in the present work. The most important (practical) omission was the behaviour in waves. Given that advanced lightweight materials are still being developed for use in high-speed vessels it is likely that a complete understanding of wave effects on ship structures will take many decades.

In the interests of brevity, several hydrodynamic aspects of the performance of high-speed vessels were omitted from consideration. Dynamic sinkage and trim are known to play an important role in the performance of some high-speed vessels, as do shallow water effects. Recent work on these topics can be found in the reports by Tuck, Scullen and Lazauskas [75], [76].

High-speed vessels can create very large waves that are potentially hazardous to other users of waterways. Previous work on this topic includes several reports and papers co-authored by the present author, see for example [70], [73], [74], [75], [76], [77], [78] and [79].

References

[1] Barratt, M.J., "The wave drag of a hovercraft", *Journal of Fluid Mechanics*, Vol. 22, part 1, 1965, pp. 39–47.

[2] Bessho, M., "On the problem of the minimum wave-making of ships", Memoirs of the Defence Academy of Japan, Vol. 2, 1962, pp. 1–30.

[3] Broadbent, Chris and Kennell, Colen, "Monohull, catamaran, trimaran and SES high speed sealift vessels", Sixth Int. Conf. on Fast Sea Transportation, ("FAST'01"), Southampton, UK, pp. 23–33, 2001.

[4] Couser, P.R., Wellicome, J.F., and Molland, A.F., "An improved method for the theoretical prediction of the wave resistance of transom-stern hulls using a slender body approach", *International Shipbuilding Progress*, Vol. 45, 1998, pp. 331–349.

[5] Crowder, W.S., Di Fiore, M.F., Dipper, M., and Dunne, G., "High speed sealift platform evaluation and analysis – Spring 98: The INCAT 046", Centre for the Commercial Development of Transport Technolgies Report, 1998.

[6] Date, J.C. and Turnock, J.C, "Computational fluid dynamics estimation of skin friction experienced by a plane moving through water", *Trans. RINA*, 2000, pp. 116–135.

[7] Dawkins, Richard, "The Selfish Gene", Oxford University Press, 1976.

[8] Day, Sandy, Clelland, David and Nixon, Edd, "Experimental and numerical investigation of 'Arrow' trimarans", Seventh Int. Conf. on Fast Sea Transportation ("FAST'03"), Ischia, Italy, pp. 23–30, 2003.

[9] Day, A.H., Doctors, L.J., and Armstrong, N.A., "Concept evaluation for large very-high-speed vessels", Fourth Int. Conf. on Fast Sea Transportation ("FAST'97"), Sydney, Australia, pp. 65–75, 1997.

[10] Delhommeau, Gerard, "Calculation of wave resistance of surface effect ships", *Schiffstechnik*, Vol. 41, 1994, pp. 149–159.

[11] Dhawan, Satish, "Direct measurements of skin-friction", NACA Technical Report 1121, 1958, pp. 281–300.

[12] Dhingra, A. K., and Lee, B.H., "A genetic algorithm approach to single and multiobjective structural optimization with discrete continuous variables", Int. J. Num. Meth. Eng., Vol. 37, pp. 4059-4080, 1994.

[13] Doctors, L. J., "On the use of pressure distributions to model the hydrodynamics of air-cushion vehicles and surface-effect ships", *Naval Engineers Journal*, Vol. 105, March 1993, pp. 69–89.

[14] Doctors, L.J., "Comments on resistance of different concepts", High-speed sealift technology workshop, High-speed hull forms and propulsor technology workgroup, Washington, DC, 4pp, Oct. 1997.

[15] Doctors, L. J., "Optimal pressure distributions for river-based air-cushion vehicles", *Schiffstechnik*, Vol. 44, 1997, pp. 32–36.

[16] Doctors, L.J. and Day, A.H., "Resistance optimization of displacement vessels on the basis of principal parameters", *Journal of Ship Research*, Vol. 41, No. 4, 1997, pp 249–259.

[17] Doctors, L.J. and Day, A.H., "Hydrodynamically optimal hull forms for river ferries", *Int. Symposium on High-Speed Vessels for Transport and Defence*, RINA, London, England, Nov. 23–24, 1995.

[18] Doctors, L.J. and Day, A.H., "Wave-free river-based air-cushion vehicles", *Proc. International Conference on Hydrodynamics of High-Speed Craft Wake Wash and Motions Control*, London, Nov. 2000.

[19] Doctors, L.J. and Day, A.H., "Steady-state hydrodynamics of high-speed vessels with a transom stern", *Proc. 23rd Symp. on Naval Hydrodynamics*, Val de Reuil, France, Sept. 2000.

[20] Doctors, L.J. and Sharma, S.D., "The wave resistance of an air-cushion vehicle in steady and accelerated motion", *Journal of Ship Research*, Vol. 16, No. 4, Dec. 1972, pp. 248–260.

[21] Eames, M.C. and Drummond, T.G., "Concept exploration - an approach to small warship design", *Trans. RINA* , 1976, pp. 29–54.

[22] Eshelman, Larry J., "The CHC adaptive search algorithm: how to have safe search when engaging in nontraditional genetic recombination", Foundations of Genetic Algorithms, Rawlins, G. J. E. (ed.), San Mateo, CA, Morgan Kaufmann, 1991, pp. 265-283.

[23] Eshelman, Larry J. and Schaffer, J. David, "Preventing premature convergence in genetic algorithms by preventing incest", Proc. Fourth Int. Conference on Genetic Algorithms and their Applications, Belew, R. and Booker, L. (eds), Morgan Kaufmann 1991.

[24] Everest, J.T. and Hogben, N., "Research on hovercraft over calm water", *Trans. RINA*, 1967, pp. 311–326.

[25] Filon, L.N.G., "On a quadrature formula for trigonometric integrals", *Proceedings of the Royal Society of Edinburgh*, Vol. 49, 1929, pp. 38–47.

[26] Gadd, G.E., "A new turbulent friction formulation based on a reappraisal of Hughes' results", *Trans. RINA*, Vol. 109, 1967, pp. 511–539.

[27] Granville, P.S., "The viscous resistance of surface vessels and the skin friction of flat plates", *Trans. SNAME*, Vol. 64, 1956, pp. 209–240.

[28] Granville, Paul S., "Drag and turbulent boundary layer of flat plates at low Reynolds numbers", *Journal of Ship Research*, Vol. 21, No. 1, March 1977, pp. 30–39.

[29] Grigson, C.W.B., "An accurate smooth friction line for use in performance prediction", *Trans. RINA*, 1993, pp. 149–152.

[30] Grigson, C.W.B., "Note on an accurate turbulent velocity profile for use at ship scale", *Journal of Ship Research*, Vol. 33, No. 3, Sept. 1989, pp. 162–168.

[31] Grigson, C.W.B., "A planar friction algorithm and its use in analysing hull resistance", *Trans. RINA*, 2000, pp. 76–115.

[32] Havelock, T.H., "Studies in wave resistance: influence of the form of the water-plane section of the ship", *Proc. Royal Society, A*, Vol. 103, 1934, pp. 571–585.

[33] Havelock, T.H., "Wave patterns and wave resistance", *Trans. RINA,* , 1934, pp. 430–442.

[34] Hearn, Grant E., Veldhuis, Ivo J.S., van't Veer, Riaan and Steenbergen, Robert Jan, "Conceptual design investigations of a very high speed trans-Pacific container ship", *Sixth Int. Conf. on Fast Sea Transportation ("FAST'01")*, Vol. 2, pp. 81–108, Southampton, England, Sept. 2001.

[35] Jones, David I.G., "Hovering performance of plenum chamber GEMS over land and water", *J. Aircraft,* Vol. 3, No. 4, 1966, pp. 333–338.

[36] Karayannis, A.F., Molland, A.F. and Sarac Williams, Y., "Design data for high-speed vessels", Fifth Int. Conf. on Fast Sea Transportation ("FAST'99"), Seattle, USA, pp. 605–615, 1999.

[37] Lavis David R. and Forstell, Brian G., "The cost-benefit of emerging technologies using physics-based ship-design synthesis", Band, Lavis and Associates, Maryland USA, 1999, pp. 13.

[38] Lazauskas, L. and Jones, K.C., "Destroyer hull resistance optimisation study", *Australian Dept. of Defence Contract No. 4500103283,* , 2002.

[39] Lazauskas, L. and Tuck, E.O., "Low drag multihulls for sporting, commercial and military applications", *Fourth Int. Conf. on Fast Sea Transportation ("FAST97")*, pp. 647–652, Baird Publications, Melbourne.

[40] Lazauskas, L. and Tuck, E.O., "Small low drag, solar-powered monohulls and multihulls", *RINA Newsletter*, July 1997.

[41] Lazauskas, L. and Tuck, E.O., "Wave cancellation by Weinblum-type catamarans and diamond-shaped tetrahulls", *EMAC98*, pp. 299–302.

[42] Maruo, H., (In Japanese), Journal of the Society of Naval Architects of Japan, Vol. 81, 1949.

[43] McKesson, C.B., "Hull form and propulsor technology for high speed sealift", Report for high-speed sealift technology workshop, John. J. McMullen Assoc. Inc, Washington, USA, 13 Feb. 1998.

[44] McKesson, C.B., "Fast ship white paper number 1", High-speed sealift technology workshop, High-speed hull forms and propulsor technology workgroup, Washington, DC, 3pp, October 1997.

[45] McKesson, C.B., "Alternative powering for merchant ships: Task 1 - Current and Forecast Powering Needs", Centre for the Commercial Development of Transport Technolgies, 2001.

[46] McKesson, C.B., "Alternative powering for merchant ships: Task 2 - Survey of available alternative powerplants for container ships", Centre for the Commercial Development of Transport Technolgies, 2002.

[47] Michell, J.H., "The wave resistance of a ship." *Philosophical Magazine*, Series 5, Vol. 45, 1898, pp. 106–123.

[48] Molland, A.F., Wellicome, J.F. and Couser, P.R., "Resistance experiments on a systematic series of high speed displacement catamaran forms: variation of length-displacement ratio and breadth-draught ratio", University of Southhampton, Ship Science Report 71, 1994.

[49] Munro-Smith, R., "Elements of Ship Design", 1975.

[50] Newman, J.N. and Poole, F.A.P., "The wave resistance of a moving pressure distribution in a canal", *Schiffstechnik*, Vol. 9, 1962, pp. 1–6.

[51] Parsons, Michael G., Singer, David J. and Sauter, John A., "A hybrid agent approach for set-based conceptual ship design", Int. Conference on Computer Applications in Shipbuilding, Cambridge, Mass. USA, June 7–11, 1999.

[52] Ranocchia, D., "22nd ITTC Specialist Committee for Model Tests of High Speed Marine Vehicles", Final Report, 1999, 40 pp.

[53] Ritter, Owen .K., and Templeman, Michael, T., "High-Speed Sealift Technology, Volume. 1", Technology Projection Report CDNSWC-TSSD-98-009, Carderock Division, Naval Surface Warfare Center, Sept. 1998, pp. 59.

[54] Schetz, Joseph A., *Foundations of boundary layer theory for momentum, heat and mass transfer*, 1st ed., 1984, Prentice–Hall.

[55] Schlichting, H., *Boundary layer theory*, 8th ed., 2000, Springer–Verlag.

[56] "U.S. Navy Salvage Engineer's Handbook, Vol 1, (Salvage Engineering)", Naval Sea Systems Command, 1994.

[57] Scragg, Carl A. and Nelson, Bruce D., "The design of an eight-oared rowing shell", *Marine Technology*, Vol. 30, No. 2, April 1993, pp. 84–99.

[58] Sharma, S.D., "Some results concerning the wavemaking of a thin ship", *Journal of Ship Research*, March 1969, pp. 72–81.

[59] Sirvio, Jari and Ahlgren, Niklas, "Large slender monohulls for fast freight carriers", Fifth Int. Conf. on Fast Sea Transportation ("FAST'99"), Seattle, USA, 1999, pp. 657–671.

[60] Smith, Donald W. and Walker, John H., "Skin-friction measurements in incompressible flow", NACA Technical Note 4231, 1958.

[61] Tatinclaux, J.C., "On the wave resistance of surface-effect ships", *Trans. SNAME*, 1975, pp. 51–66.

[62] Trillo, Robert, L., "High speed over water, ideas from the past, the present and for the future", First Int. Conf. on Fast Sea Transportation ("FAST'91"), Trondheim, Norway, pp. 17–34, 1991.

[63] Tselnik, D.S., "On the jet curtain over water", *Journal of Ship Research*, Vol. 26, No. 2, June 1982, pp. 77–88.

[64] Tuck, E.O., Collins, J.L. and Wells, W.H., "On ship waves and their spectra", *Journal of Ship Research*, Vol. 15, March 1971, pp. 11–21.

[65] Tuck, E.O., "Wave resistance of thin ships and catamarans", Report T8701, Applied Mathematics Department, The University of Adelaide, 1987.

[66] Tuck, E.O., "The wave resistance formula of J.H. Michell (1898) and its significance to recent research in ship hydrodynamics", Journal of the Australian Mathematical Society, Series B 30, 1989, pp. 365–377.

[67] Tuck, E.O., "Can lateral asymmetry of the hulls reduce catamaran wave resistance?", 20th Int. Workshop on Water Waves and Floating Bodies, Spitzbergen, May 2005 (submitted).

[68] Tuck, E.O. and Lazauskas, L., "Low drag rowing shells", 3rd Conf. on mathematics and computers in sport, Bond University, Queensland, Australia, 30 Sept. 1996 - 2nd Oct. 1996.

[69] Tuck, E.O. and Lazauskas, L., "Unconstrained ships of minimum total drag", Applied Mathematics Department, The University of Adelaide, Dec. 1996.

[70] Tuck, E.O. and Lazauskas, L., "Optimum spacing of a family of multihulls", *Schiffstechnik*, Vol. 45, 1998, pp. 180–195.

[71] Tuck, E.O. and Lazauskas, L., "Polymich", Department of Applied Mathematics, The University of Adelaide, 1999.

[72] Tuck, E.O. and Lazauskas, L., "Free-surface pressure distributions with minimum wave resistance", *ANZIAM Journal*, Vol. 43, 2001, pp. E75–E101.

[73] Tuck, E.O., Scullen, D.C. and Lazauskas, L., "Sea Wave Pattern Evaluation, Part 1 report: Primary code and test results", Applied Mathematics Department, The University of Adelaide, April 1999.

[74] Tuck, E.O., Scullen, D.C. and Lazauskas, L., "Sea Wave Pattern Evaluation, Part 3 report: Near-field waves", Applied Mathematics Department, The University of Adelaide, Jan. 2000.

[75] Tuck, E.O., Scullen, D.C. and Lazauskas, L., "Sea Wave Pattern Evaluation, Part 4 report: Extension to multihulls and finite depth", Applied Mathematics Department, The University of Adelaide, June 2000.

[76] Tuck, E.O., Scullen, D.C. and Lazauskas, L., "Sea Wave Pattern Evaluation, Part 5 report: Speed-up and squat", Applied Mathematics Department, The University of Adelaide, March 2001.

[77] Tuck, E.O., Scullen, D.C. and Lazauskas, L., "Sea Wave Pattern Evaluation, Part 6 report: Viscosity factors", The University of Adelaide, Jan. 2002.

[78] Tuck, E.O., Scullen, D.C. and Lazauskas, L., "Ship-wave patterns in the spirit of Michell", *Proceedings of the IUTAM Symposium on Free-Surface Flows*, Birmingham, July 2000, ed. A.C. King and Y.D. Shikhmurzaev, Kluwer Academic Publishers, Dordrecht, 2001, pp. 311–318.

[79] Tuck, E.O., Scullen, D.C. and Lazauskas, L., "Wave patterns and minimum wave resistance for high-speed vessels", 24th Symposium on Naval Hydrodynamics, Fukuoka, JAPAN, July 2002.

[80] Voigt, H.M., "Soft genetic operators in evolutionary algorithms", in W. Banzhaf and F.H. Eeckmann (eds): Evolution and Biocomputation, Lecture Notes in Computer Science 899, pp. 123-141, Springer, Berlin, 1995

[81] Watson, D.G.M. and Gilfillan, A.W., "Some ship design methods", *Trans. RINA*, 1977, pp. 279–324.

[82] Wehausen, J.V. and Laitone, E.V., *Surface Waves*, in Handbuch der Physik, ed. Flügge S., Chapter 9, Springer-Verlag, 1962.

[83] Wehausen, John V., "The wave resistance of ships", Advances in Applied Mechanics, Vol. 13, 1973, pp. 93–245.

[84] Yim, Bohyun, "On the wave resistance of surface effect ships", *Journal of Ship Research*, Vol. 15, No. 1, March 1971, pp. 22–32.